



The myelin content of the human precentral hand knob reflects inter-individual differences in manual motor control at the physiological and behavioural level

Dubbioso, Raffaele; Madsen, Kristoffer Hougaard; Thielscher, Axel; Siebner, Hartwig Roman

Published in:
Journal of neuroscience

Link to article, DOI:
[10.1523/JNEUROSCI.0390-20.2021](https://doi.org/10.1523/JNEUROSCI.0390-20.2021)

Publication date:
2021

Document Version
Peer reviewed version

[Link back to DTU Orbit](#)

Citation (APA):
Dubbioso, R., Madsen, K. H., Thielscher, A., & Siebner, H. R. (2021). The myelin content of the human precentral hand knob reflects inter-individual differences in manual motor control at the physiological and behavioural level. *Journal of neuroscience*, 41(14), 3163-3179. <https://doi.org/10.1523/JNEUROSCI.0390-20.2021>

General rights

Copyright and moral rights for the publications made accessible in the public portal are retained by the authors and/or other copyright owners and it is a condition of accessing publications that users recognise and abide by the legal requirements associated with these rights.

- Users may download and print one copy of any publication from the public portal for the purpose of private study or research.
- You may not further distribute the material or use it for any profit-making activity or commercial gain
- You may freely distribute the URL identifying the publication in the public portal

If you believe that this document breaches copyright please contact us providing details, and we will remove access to the work immediately and investigate your claim.

Research Articles: Systems/Circuits

The myelin content of the human precentral hand knob reflects inter-individual differences in manual motor control at the physiological and behavioural level

<https://doi.org/10.1523/JNEUROSCI.0390-20.2021>

Cite as: J. Neurosci 2021; 10.1523/JNEUROSCI.0390-20.2021

Received: 18 February 2020

Revised: 22 February 2021

Accepted: 24 February 2021

This Early Release article has been peer-reviewed and accepted, but has not been through the composition and copyediting processes. The final version may differ slightly in style or formatting and will contain links to any extended data.

Alerts: Sign up at www.jneurosci.org/alerts to receive customized email alerts when the fully formatted version of this article is published.

Copyright © 2021 Dubbioso et al.

This is an open-access article distributed under the terms of the Creative Commons Attribution 4.0 International license, which permits unrestricted use, distribution and reproduction in any medium provided that the original work is properly attributed.

1 **The myelin content of the human precentral hand knob reflects inter-individual differences in manual**
2 **motor control at the physiological and behavioural level**

3 Raffaele Dubbioso^{1,2*}, Kristoffer Hougaard Madsen^{1,3}, Axel Thielscher^{1,4}, Hartwig Roman Siebner^{1,5,6*}

4 ¹Danish Research Centre for Magnetic Resonance, Centre for Functional and Diagnostic Imaging and
5 Research, Copenhagen University Hospital Hvidovre, Hvidovre, Denmark

6 ²Department of Neurosciences, Reproductive Sciences and Odontostomatology, University Federico II of
7 Naples, Naples, Italy.

8 ³Department of Applied Mathematics and Computer Science, Technical University of Denmark, Kgs.
9 Lyngby, Denmark.

10 ⁴Department of Health Technology, Technical University of Denmark, Kgs. Lyngby, Denmark.

11 ⁵Department of Neurology, Copenhagen University Hospital Bispebjerg, Copenhagen, Denmark.

12 ⁶Institute for Clinical Medicine, Faculty of Health and Medical Sciences, University of Copenhagen,
13 Copenhagen, Denmark

14

15 **Short title:** Structure-function relationships in the precentral motor hand knob

16 **Word count:** Abstract: 250; Introduction: 759; Discussion: 2864

17 **Number of figures:** 7; **Tables:** 1

18 ***Corresponding authors**

19 Raffaele Dubbioso, MD, PhD

20 Department of Neurosciences, Reproductive Sciences and Odontostomatology, University Federico II of
21 Napoli, Via Sergio Pansini, 5. 80131 Napoli, Italy.

22 Phone: +39 081 7464579. e-mail: rafdubbioso@gmail.com

23 Hartwig R. Siebner, MD, DMSc

24 Danish Research Centre for Magnetic Resonance (DRCMR), Center for Functional and Diagnostic Imaging
25 and Research, Copenhagen University Hospital Hvidovre, Kettegård Allé 30, DK-2650 Hvidovre, Denmark.

26 Phone: +45 3862 6541 -, e-mail: h.siebner@drcmr.dk

27 Acknowledgments

28 We thank Sofie Johanna Nilsson for helping with the acquisition of MRI data. We are grateful to Lasse
29 Christiansen, Peter Jagd Sørensen, Silas Haahr Nielsen, Estelle Raffin and Johannes Stelzer for data
30 analysis and comments on the manuscript. We would like to thank Antoine Lutti, Gunther Helms, and
31 Nikolas Weiskopf for providing the multiparameter MRI sequence which was used to obtain quantitative
32 R1 maps.

33

34 Author Contributions

35 R.D. designed the study, acquired, pre-processed, analysed and interpreted the data, and drafted a first
36 version of the manuscript.

37 K.H.M. designed the study, participated in analysis and interpretation of the data

38 A.T. designed the study, participated in analysis and interpretation of the data

39 H.R.S. designed the study, participated in interpretation of the data and in drafting a first version of the
40 manuscript.

41

42 Conflict of Interest

43 Hartwig R. Siebner has received honoraria as speaker from Sanofi Genzyme, Denmark and Novartis,
44 Denmark, as consultant from Sanofi Genzyme, Denmark and Lundbeck AS, Denmark, and as editor-in-chief
45 (Neuroimage Clinical) and senior editor (NeuroImage) from Elsevier Publishers, Amsterdam, The
46 Netherlands. He has received royalties as book editor from Springer Publishers, Stuttgart, Germany and from
47 Gyldendal Publishers, Copenhagen, Denmark. The other authors report no conflict of interests.

48

49 Funding

50 This work is part of the project “Biophysically adjusted state-informed cortex stimulation” (BASICS) funded
51 by a synergy grant from Novo Nordisk Foundation (Interdisciplinary Synergy Program 2014; grant number
52 NNF14OC001. Hartwig R. Siebner holds a 5-year professorship in precision medicine at the Faculty of
53 Health Sciences and Medicine, University of Copenhagen which is sponsored by the Lundbeck Foundation
54 (Grant Nr. R186-2015-2138).

55

56 **Abstract**

57 The primary motor hand area ($M1_{\text{HAND}}$) and adjacent dorsal premotor cortex (PMd) form the so-called motor
58 hand knob in the precentral gyrus. $M1_{\text{HAND}}$ and PMd are critical for dexterous hand use and are densely inter-
59 connected via cortico-cortical axons, lacking a sharp demarcating border. In 24 young right-handed
60 volunteers, we performed multi-modal mapping to delineate the relationship between structure and function
61 in the right motor hand knob. Quantitative structural magnetic resonance imaging (MRI) at 3 Tesla yielded
62 regional $R1$ -maps as a proxy of cortical myelin content. Participants also underwent functional MRI. We
63 mapped task-related activation and temporal precision, while they performed a visuo-motor synchronization
64 task requiring visually cued abduction movements with the left index or little finger. We also performed
65 sulcus-aligned transcranial magnetic stimulation (TMS) of the motor hand knob to localize the optimal site
66 (hotspot) for evoking a motor evoked potential (MEP) in two intrinsic hand muscle. Individual motor hotspot
67 locations varied along the rostro-caudal axis. The more rostral the motor hotspot location in the precentral
68 crown, the longer were corticomotor MEP latencies. “Hotspot rostrality” was associated with the regional
69 myelin content in the precentral hand knob. Cortical myelin content also correlated positively with task-
70 related activation of the precentral crown and temporal precision during the visuo-motor synchronization
71 task. Together, our results suggest a link between cortical myelination, the spatial cortical representation and
72 temporal precision of finger movements. We hypothesize that the myelination of cortical axons facilitates
73 neuronal integration in PMd and $M1_{\text{HAND}}$ and hereby, promotes the precise timing of movements.

74

75

76 **Significance statement**

77 Here we used magnetic resonance imaging and transcranial magnetic stimulation (TMS) of the precentral
78 motor hand knob to test for a link between cortical myelin content, functional cortico-motor representations,
79 and manual motor control. A higher myelin content of the precentral motor hand knob was associated with
80 more rostral corticomotor presentations, with stronger task-related activation and a higher precision of
81 movement timing during a visuo-motor synchronization task. We propose that a high precentral myelin
82 content enables fast and precise neuronal integration in M1 and PMd, resulting in higher temporal precision
83 during dexterous hand use. Our results identify the degree of myelination as an important structural feature
84 of the neocortex that is tightly linked to the function and behaviour supported by the cortical area.

85

86 **Keywords:** motor skill, premotor cortex, primary motor cortex, functional cortical mapping, magnetic
87 resonance imaging.

88

89

90

91 **Introduction**

92 The primary motor hand area ($M1_{\text{HAND}}$) and adjacent dorsal premotor cortex (PMd) are critical for dexterous
93 hand use in human and non-human primates. The $M1_{\text{HAND}}$ enables the independent use of single fingers
94 through direct cortico-motoneuronal control of hand and finger muscles (Lemon, 2008, 2019). The rostral
95 (“old”) and caudal (“new”) parts of $M1_{\text{HAND}}$ differ with respect to their cortico-motoneuronal connectivity
96 (Rathelot and Strick, 2006, 2009; Witham et al., 2016). Only the caudal $M1_{\text{HAND}}$ which is located deep in the
97 anterior wall of the precentral sulcus contains large, fast-conducting pyramidal cells that produce short-
98 latency monosynaptic responses in spinal motoneurons. The rostral part of $M1_{\text{HAND}}$ (and the somatosensory
99 area 3a) exert descending motor control over cervical spinal motoneurons via more slowly conducting
100 monosynaptic as well as di-synaptic projections (Witham et al., 2016). The PMd also plays an important role
101 in manual motor control, contributing to the selection and execution of hand and finger movements (Picard
102 and Strick, 2001; Ward et al., 2010). Its prominent role is reflected by dense reciprocal connections with
103 $M1_{\text{HAND}}$ (Dum and Strick, 2005) and by the fact that the most caudal part of PMd contains scattered large
104 pyramidal cells which send axonal projections to the cervical cord via the pyramidal tract (Geyer et al.,
105 2000).

106 The $M1_{\text{HAND}}$ and PMd form a characteristic knob-like structure in the human precentral gyrus (Yousry et al.,
107 1997). The precentral motor hand knob can be easily identified by structural magnetic resonance imaging
108 (MRI) due to its visible omega or epsilon shape (Yousry et al., 1997). The $M1_{\text{HAND}}$ and PMd lack a clear
109 anatomical demarcation line. Cytoarchitectonic mapping studies showed that the rostral border of the
110 primary motor cortex extends to the surface of the precentral crown close to the midline, but retracts to the
111 rostral bank of the central sulcus in more lateral parts of the hemisphere (Geyer et al., 1996, 2000). The
112 caudal PMd occupies most of the crown and lip of the precentral hand region and belongs cyto-
113 architectonically to Brodmann area 6 (BA6). However, the transition between rostral $M1_{\text{HAND}}$ and caudal
114 PMd is smooth and there is subject inter-individual variability regarding the rostral extension of the $M1_{\text{HAND}}$
115 (Geyer et al., 1996, 2000). In agreement with a smooth cytoarchitectonic transition, the dendritic tree of
116 supragranular (layer III) pyramidal cells in the precentral cortex of macaques becomes gradually more
117 complex with rostral progression from the central sulcus (M1) to adjacent premotor cortex (Elston and
118 Rockland, 2002).

119 The physiology of the precentral motor hand knob and its corticomotor output to the contralateral hand can
120 be studied in humans with transcranial magnetic stimulation (TMS) (Barker et al., 1985; Palmer and Ashby,
121 1992; Maertens De Noordhout et al., 1999; Groppa et al., 2012). The site to target M1_{HAND} is functionally
122 defined as the site where TMS elicits the largest motor evoked potential (MEP) in contralateral hand
123 muscles, commonly referred to as “motor hotspot” (Groppa et al., 2012; Rossini et al., 2015). But TMS can
124 also be used to map the functional topography of corticomotor representations by applying TMS at different
125 scalp positions using a two-dimensional grid (Wassermann et al., 1993; Pascual-Leone et al., 1994; Veldema
126 et al., 2017). TMS-based corticomotor mapping has consistently shown substantial inter-individual variations
127 in precentral motor hotspot location along the anterior-posterior grid axis (Teitti et al., 2008; Diekhoff et al.,
128 2011; Vaalto et al., 2011; Sarfeld et al., 2012; Ahdab et al., 2014, 2016).

129 Post-mortem myeloarchitectonic analyses have shown that the precentral gyrus is one of the cortical areas
130 which contains the highest density of myelinated axons (Nieuwenhuys, 2013). Using myelin-sensitive read-
131 outs (Glasser and van Essen, 2011; Lutti et al., 2014), in vivo magnetic resonance imaging (MRI) confirmed
132 that the myelin content in the frontal cortex peaks in the pericentral gyrus and then gradually decreases along
133 a posterior-anterior gradient (Glasser and van Essen, 2011). MRI-based cortical myelin mapping also
134 revealed considerable inter-individual variability (Shams et al., 2019) with respect to the regional myelin
135 content. Since myelination enables fast signal propagation and synchronizes neural activity (Seidl et al.,
136 2010; Pajevic et al., 2014; Ford et al., 2015; Timmler and Simons, 2019), the degree of precentral
137 myelination may account for functional phenotypic variation in precentral cortical function and dexterous
138 hand use. To test this hypothesis, we combined structural myelin-sensitive MRI, task-related functional
139 MRI, with a novel sulcus-aligned TMS mapping approach. We reasoned that our multimodal mapping
140 approach can reveal structural and functional features in the precentral gyrus that may account for inter-
141 individual variability regarding the evoked corticomotor responses and contribute to inter-individual
142 differences in the plasticity-inducing effects of repetitive TMS on corticomotor excitability.

143

144 **Materials and methods**

145 **Participants and power analysis**

146 Our main goal was to detect a link between regional cortical myelination and a read-out of corticomotor
147 representation as revealed by our novel TMS mapping procedure (see below for details). Since this novel
148 TMS-based measure (i.e., rostrality index) had not been used in previous work, we could not perform a
149 proper power analysis. We therefore based our sample size estimation on previous neurophysiological TMS
150 mapping studies. Here, the number of participants included in a single study ranged from 11 to 17 healthy
151 volunteers (Teitti et al., 2008; Diekhoff et al., 2011; Vaalto et al., 2011, 2016; Sarfeld et al., 2012; Ahdab et
152 al., 2014, 2016). We decided to recruit 24 participants to secure a sample size that exceeded previous TMS
153 mapping studies, factoring in an estimated drop-out rate of 20%.

154 Twenty-four healthy young adults (12 women and 12 men) with a mean age of 24 years, ranging from 19 to
155 34 years, and a mean height of 173 cm (range: 163-187 cm) participated in this study. Participants were
156 consistently right-handed as assessed by the Edinburgh handedness inventory (Oldfield, 1971). Only
157 individuals with little (<2 years) or no formal music training were included. They had no previous history of
158 neurological or psychiatric disorders and were screened for contraindications to TMS (Rossi et al., 2009).
159 They all gave written informed consent to the experimental procedures. The study complied with the
160 Helsinki declaration on human experimentation and was approved by the Ethical Committee of the Capital
161 Region of Denmark (H-15000551).

162

163 **Experimental procedures and data acquisition**

164 Experimental procedures are illustrated in Fig.1 and comprise corticomotor TMS mapping as well as
165 structural and functional magnetic resonance (MRI) of the whole brain at 3 tesla. All participants underwent
166 structural and functional MRI the day before the TMS mapping experiment. All MRI scans were acquired
167 with a 3 T Verio Scanner and a 32-channel head coil (Siemens, Erlangen, Germany).

168

169 **Structural MRI**

170 Structural T1-weighted images were acquired to assess cortical thickness and to individually identify and
171 track the TMS-target points with frameless stereotactic neuronavigation on each participant's
172 macrostructure. The T1-weighted images had an isotropic resolution with a voxel size of 1mm³ (TR = 2300

173 ms, TE = 2.96 ms, flip angle = 9°). T2-weighted images were acquired to inform offline simulation of the
174 induced electric fields in the precentral gyrus in each individual participant given the intensity of the
175 stimulation and the distance of the coil from the scalp in each condition. T2-weighted whole-brain scans had
176 a voxel size of 1x1x2 mm³ (TR = 10000ms, TE = 52ms, flip angle= 120°). In addition, a whole-brain
177 multiparameter mapping protocol was run to obtain quantitative R1 maps as an index of regional cortical
178 myelination (Helms et al., 2008; Lutti et al., 2010). The protocol is based on multi-echo 3D Proton Density-
179 and T1-weighted FLASH (fast low angle shot) images at 1 mm isotropic resolution, which undergo
180 correction for radio frequency (RF) transmit field inhomogeneities using an EPI (echo-planar imaging)-based
181 B1+ map. The latter is corrected for off-resonance effects using a B0 field map. For further details regarding
182 the sequence parameters, we refer to two publications (Weiskopf and Helms, 2008; Weiskopf et al., 2011).

183

184 **Functional MRI**

185 Functional MRI used a gradient-echo planar imaging (EPI) sequence sensitive to detect task-related blood-
186 oxygenation level dependent (BOLD) changes in tissue contrast (TR = 2.07 s, TE = 30 ms, flip angle = 78°,
187 voxel size = 2×2×2 mm³, axial field of view = 192×192 mm). A single brain volume consisted of 25 axial
188 slices covering the upper half of the brain. The axial orientation of the brain volumes orientation was slightly
189 tilted backwards so that the orientation of the slices was approximately perpendicular to the course of the
190 central sulcus. 335 brain volumes were acquired during the fMRI session. Two additional short whole-brain
191 EPI scans (62 slices) with the same parameters except for an adjusted TR were recorded for co-registration
192 purposes. Pulse and respiration were recorded with an infrared pulse oximeter and a pneumatic thoracic belt.
193 Task related activity changes were mapped with BOLD fMRI while participants performed a repetitive
194 isometric finger abduction task with their left index or little finger (Fig.1D). This task engaged the same
195 muscles that were investigated with TMS, namely the FDI and ADM muscle. The left hand of the subject
196 was placed on a board fitted with two strain gauge sensors measuring the abduction forces produced with the
197 index or little finger (Fig.1D). The strain gauges sensors were connected to a custom amplifier which
198 converted the measured force to a voltage in the range 0-2.5 V, this signal was sampled via a PicoLog 1216
199 USB 2.0 acquisition device at a sampling rate of 500 Hz. Involuntary movement of the thumb, the middle
200 and the ring finger were avoided by using adhesive felt. Subjects saw a schematic drawing of the back of the

201 left hand displayed on a video screen that was visible to the subjects via a coil-mounted mirror. Red or green
202 dots were presented every second at the tip of the left index or little finger. Participants had to produce an
203 isometric abduction with the corresponding finger, whenever a green dot appeared at the tip of the target
204 finger. Participants had to refrain from any movement, whenever a red dot was presented. Using a block
205 design, the same dot and colour was presented 10 times. The duration of presentation of green or red dots
206 within each block was 0.5 s at a constant frequency of 1 Hz without any jitter. The visuo-motor
207 synchronization task consisted of blocks of movements (green dots) alternated with blocks without
208 movements (red dots). The four task conditions were always performed in a fixed order and repeated 18
209 times during the fMRI run (Fig.1D). Stimulus presentation and response recording was controlled by
210 custom-made programs (PsychoPy software, v. 1.74.01, www.psychopy.org) (Peirce, 2009). Immediately
211 before the fMRI experiment, all participants performed a short training version of the task outside the MRI
212 scanner to get familiarized with the task. We instructed participants to emphasize on the timing of movement
213 and try to synchronize as best as possible movement rate to the pace of the visual cue to the best of their
214 ability. Performance of the subjects in the scanner was controlled by video monitoring. Importantly, we were
215 interested in movement regularity and synchronization to visual inputs, rather than in the accuracy of
216 responding with the correct finger or producing a constant abduction force. Therefore, our task probed visuo-
217 to-motor synchronization of simple repetitive finger movements rather than visuo-to-motor response
218 mapping. We reasoned that the degree of cortical myelination in the precentral hand knob should scale with
219 temporal precision of movement (i.e., the ability to reliably adjust movement repetition rate to the pace of the
220 external cue). Therefore, we hypothesized that high levels of precentral cortical myelination should be
221 associated with low trial-to-trial variability of the between-movement interval during the visually cued
222 movement synchronization task.

223

224 **Transcranial magnetic stimulation**

225 We applied a sulcus-aligned TMS mapping approach that has been developed by our group (Raffin et al.,
226 2015; Dubbioso et al., 2017; Raffin and Siebner, 2018) to precisely localize the optimal site for evoking
227 MEPs in two intrinsic hand muscles (i.e., precentral motor hotspot) along the rostro-caudal axis in the crown
228 of the precentral gyrus (Fig.1). Single biphasic TMS pulses were applied over multiple sites overlaying the

229 right precentral hand knob. TMS was performed with a cooled MC-B35 figure-of-eight coil connected to a
230 MagPro X100 stimulation device (Magventure, Farum, Denmark). We chose a MC-B35 TMS coil, because
231 this coil is small with an average winding diameter of 35 mm diameter to maximize the focality of TMS.
232 Participants were seated in an adjustable armchair with the neck supported by a head-rest during TMS
233 mapping. The position of the TMS coil relative to the participant's head was continuously tracked in real
234 time with frameless stereotactic neuronavigation (Localite GmbH, Bonn, Germany). Any changes in the
235 TMS position and orientation relative to the scalp were registered and updated online in a 3D space and
236 displayed to the examiner on a screen. Prior to sulcus-aligned TMS mapping, we located the motor hotspot
237 position of the left FDI muscle using the standard trial-and-error procedure with the handle of the coil angled
238 at 45-degree relative to the midsagittal line (Groppa et al., 2012). We then determined the resting motor
239 threshold (RMT) of the left FDI muscle, using the Maximum-Likelihood Strategy using Parameter
240 Estimation by Sequential Testing (MLS-PEST) approach (Awiszus, 2003).

241 The TMS-evoked motor responses were recorded with surface electromyography from relaxed left first FDI
242 and ADM using a belly-tendon montage (Ambu Neuroline 700, Columbia, USA). Trial-wise acquisition of
243 MEPs was controlled by Signal software and EMG data were stored on a computer for later offline analysis
244 (Cambridge Electronic Design, Cambridge, UK). Surface EMG signals were recorded at a sampling rate of
245 10 kHz and bandpass filtered (20 Hz – 3000 Hz) with an eight channel DC amplifier (1201 micro Mk-II unit,
246 Digitimer, Cambridge Electronic Design, Cambridge, UK).

247

248 **Sulcus-aligned TMS mapping of the motor hand knob**

249 Standard grid-based TMS mapping of corticomotor representations keeps the coil orientation of the TMS
250 coil identical across all grid sites (Teitti et al., 2008; Diekhoff et al., 2011; Vaalto et al., 2011, 2016; Sarfeld
251 et al., 2012; Ahdab et al., 2014, 2016). This procedure induces electrical tissue currents in the motor hand
252 knob that enter the precentral crown at different angles at the maximally stimulated part of the crown, when
253 placing the coil at different points of the grid. This is problematic because the angle at which the electrical
254 current “hits” the precentral gyrus has a strong impact on the TMS-induced electric field (Thielscher et al.,
255 2011). In addition many of these mapping studies showed considerable inter-individual variation in the

256 hotspot location, with some participants having the hot-spot located even in the pre-frontal regions (Teitti et
257 al., 2008; Vaalto et al., 2011; Ahdab et al., 2014, 2016).

258 These considerations prompted us to develop a sulcus aligned TMS mapping procedure which adjusts the
259 orientation of the TMS coil at each mapping site to the local curvature of the precentral gyrus (Raffin et al.,
260 2015; Dubbioso et al., 2017; Raffin and Siebner, 2018). The procedure exploits the fact that the motor hand
261 representation in the precentral gyrus can be readily identified on structural MRIs by its characteristic knob-
262 like shape (Yousry et al., 1997). The TMS coil is centred on one of seven equidistant target sites placed
263 along the individual gyrus-sulcus border of the hand knob. The coil orientation is adjusted at each target site
264 in a way that TMS always induces the strongest currents in a direction that is perpendicular to the local
265 orientation of the precentral gyrus. This secures that TMS induces the highest electrical field strength in the
266 crown of the precentral hand knob at all stimulation sites.

267 In this study, we extended our linear sulcus-aligned TMS mapping approach into a two-dimensional TMS
268 mapping procedure to identify inter-individual differences in the rostro-caudal peak location of corticomotor
269 excitability in the precentral gyrus. We added four parallel lines rostrally to the central sulcus over the
270 precentral gyrus (Fig.1A). Each of the five parallel lines consisted of seven equidistant targets covering the
271 entire longitudinal extension of the hand knob (35 target sites in total). The distance between two
272 neighbouring target sites on the line was 5 mm. The first two lines covered the posterior lip of the precentral
273 crown and the remaining three lines the top (apex) and anterior lip of the precentral gyral crown (Fig.1A).
274 We reasoned that a sulcus-aligned mapping approach would be more sensitive than standard grid-based
275 mapping with a conventional figure-8-coil to detect very small inter-individual variations of hotspot location.
276 Indeed, personalization to the Pre-CS shape and a short inter-line distance rendered our approach more
277 sensitive to subtle shifts in hotspot location in the Pre-CS.

278 TMS mapping was stereo-tactically guided using frameless neuronavigation (Localite GmbH, Bonn,
279 Germany). First, the head of the subject was co-registered with the individual high-resolution anatomical
280 MRI of the brain via anatomical landmarks (e.g., nasion and crus helcis) by using the surface mapping
281 function of Localite. The root mean square differences between positions of landmarks in the MRI volume
282 and at the subjects head were ≤ 2 mm for any TMS session of this study. Furthermore, to verify the quality of
283 the co-registration procedure, we attached small vitamin E capsules (providing a good MRI T1 contrast) to a

284 volunteer's head at different anatomical positions. The software depicted and true positions of the capsules
285 did not show mismatches larger than 1 mm for any position.

286 The brain surface, derived from the individual T1-weighted MRI, was rendered online and the sites to be
287 targeted by TMS in the precentral gyrus were marked as dots on the segmented brain of each subject
288 (Fig.1A). Based on anatomic landmarks, a trained investigator (R.D.) manually placed thirty-five stimulation
289 sites: seven targets for five lines. As in our recent sulcus-aligned mapping studies (Raffin et al., 2015;
290 Dubbioso et al., 2017; Raffin and Siebner, 2018), we chose a biphasic TMS pulse configuration. Biphasic
291 pulse configurations are more efficient to stimulate the M1_{HAND} than monophasic pulses (Lang et al., 2006).
292 This allowed to use of a very focal coil without any heating problems, increasing focality compared to
293 standard coils. The second phase of the biphasic stimulus always produced a current in the precentral gyrus
294 with a caudal-to-rostral (posterior-anterior) direction perpendicularly to the local curvature of the central
295 sulcus (Kammer et al., 2001).

296 To avoid carry-over effects between consecutive stimuli, inter-stimulus intervals were jittered between 4 and
297 5 s. For each target, we delivered 20 pulses in two 10-stimuli blocks at an intensity set to 120% of the
298 conventionally defined RMT for left FDI muscle. At this stimulation intensity, we reliably evoked motor
299 responses in the left FDI and ADM muscle. The order of stimulated precentral targets was pseudo-
300 randomized across subjects with a fixed target sequence within a subject. The individual coil positioning
301 parameters were stored by the neuronavigation software for each stimulation position (Localite GmbH,
302 Bonn, Germany).

303

304

305 **Data analysis**

306 **Motor evoked potentials**

307 After the experiment, the EMG recordings were visually inspected to remove trials with significant artefacts.
308 The peak-to-peak amplitude of each motor evoked potential (MEP) was extracted trial-by-trial using Signal
309 software (Signal Version 4.02 for Windows, Cambridge Electronic Design, Cambridge, UK) in the time
310 window between 10 and 40 ms after the TMS stimulus. For each of the 35 cortical targets, we determined
311 mean peak-to-peak MEP amplitude and used the mean MEP amplitude to generate muscle excitability maps

312 for the ADM and FDI muscles along the precentral gyrus (Fig.1B). The resulting map indicated the site at
313 which the mean MEP amplitude reached its peak. This “MEP peak” indicates the individual location of the
314 motor hotspot in the precentral hand knob. Please note that we used the motor hotspot location derived from
315 sulcus-shape based TMS mapping for all further analyses. The conventionally identified hotspot location that
316 we had determined by trial-and-error at the start of the experiment to determine RMT was only considered in
317 the analyses involving the simulation of the TMS-induced electrical field strength. In addition, we tested
318 stability and reproducibility of this procedure on a single subject by replicating the TMS mapping procedure
319 one week later. We used a custom-made software to extract the MNI normalized stereotactic x-, y- and z-
320 coordinates, reflecting the cortical projection of the precentral motor hotspot as revealed by our sulcus-
321 aligned mapping procedure.

322 We hypothesized that in individuals with a more rostral (anterior) precentral hotspot, TMS elicits premotor
323 cortical excitation more up-stream to MI_{HAND} than in individuals with a more posterior (caudal) precentral
324 hotspot. We therefore expected that individuals with a rostral hotspot should also show longer MEP latencies
325 than individuals with a caudal motor hotspot location in the precentral crown. Therefore, we determined the
326 shortest MEP latency for the FDI and ADM muscle for each subject at the motor hotspot location. The
327 shortest latencies were identified and measured by visual inspection of superimposed MEP waveforms (Chen
328 et al., 2008; Groppa et al., 2012). This measurement was done by an experienced neurophysiologist (PJS)
329 who was blinded with respect to the protocol set-up. We opted for corticomotor latency, because this
330 measure had been employed in previous studies (Hamada et al., 2013; Volz et al., 2015) that successfully
331 explore intra-individual effects of changing current direction on corticomotor conduction time, but
332 acknowledge that the estimation of corticomotor conduction time would have been preferable to minimize
333 the contribution of peripheral motor conduction time (Groppa et al., 2012).

334

335 **Cortical thickness, folding and myelination**

336 Cortical reconstruction was performed with the FreeSurfer image analysis suite ver. 6.0.0
337 (<http://surfer.nmr.mgh.harvard.edu/>) (Fischl and Dale, 2000). Using this approach, the grey and white matter
338 surfaces were defined by an automated brain segmentation process. If required, an experienced investigator
339 manually corrected the automated segmentation, following the procedures outlined at

340 <https://surfer.nmr.mgh.harvard.edu/fswiki/Edits>. The processes of surface extraction and inflation generated
341 a number of well-known feature descriptors for the geometry of the cortical surface. These included: surface
342 curvature estimated from the mean curvature (or average of the principal curvatures) of the white matter
343 surface (Pienaar et al., 2008); cortical thickness estimated at each point across the cortex by calculating the
344 distance between the grey/white matter boundary and the cortical surface. Individual whole brain surface
345 maps were smoothed with a 5 mm 2D Gaussian smoothing kernel (Fischl and Dale, 2000) and the effect of
346 surface curvature on cortical thickness was regressed out (Glasser et al., 2016). Using the FreeSurfer
347 spherical registration method, the individual curvature-corrected cortical thickness maps were registered to a
348 common FreeSurfer template surface (fsaverage) for visualization and group analysis (Fig.1D) (Fischl,
349 2012).

350 The data of the multiparameter mapping protocol was processed using a Voxel-Based Quantification (VBQ)
351 toolbox developed for SPM8 (www.fil.ion.ucl.ac.uk/spm/).

352 Because curvature-associated modulations of myelination can obscure or distort myelination changes due to
353 other variations in cyto- and myelo-architectonics (Annese et al., 2004), we have regressed out curvature and
354 used for analysis the curvature-corrected R1-value variations, smoothed with a 5 mm 2D Gaussian
355 smoothing kernel (Fischl and Dale, 2000). The individual maps were registered onto the FreeSurfer group
356 template for visualization and group analysis (Fig.1C).

357 We were primarily interested in estimating regional cortical myelination as reflected by R1-values
358 derived from quantitative structural MRI in the right precentral gyrus forming the motor hand knob.
359 Therefore, we defined the right motor hand knob as precentral region-of-interest (ROI), covering the M1_{HAND}
360 and the adjacent PMd directly anterior to it. Within this ROI, we separately defined the Caudal Pre-Central
361 Gyrus (Pre-CG), namely the gyral wall facing the central sulcus and the Rostral Pre-CG, the gyral crown and
362 gyral wall facing Pre-central sulcus. The border between the Caudal and the Rostral Pre-CG was manually
363 delineated on the average group image generated in freesurfer by using a line perpendicular to the cortical
364 surface originating at the maximal convexity of the posterior lip region.

365 Then, the medio-lateral and antero-posterior borders of the overall ROI were defined based on the grid we
366 used for precentral TMS mapping to achieve a reliable comparison of the MRI and TMS data. First, we
367 considered the border of the grid by taking the grand mean of MNI normalized stereotactic x-, y- and z-

368 coordinates of the stimulation points forming the grid border of all participants. These coordinates were then
369 projected on the flat FreeSurfer template surface (fsaverage) by using a custom-made matlab script. Each
370 point was then connected to form a rectangle with a size of approximately 2 x 3 cm, using the function
371 `tksurfer_labeledit` implemented in the FreeSurfer software package. The rectangle was finally projected onto
372 the pial surface (Fig. 2A). Individual mean cortical thickness values and R1-based cortical myelination
373 estimates were extracted from the two precentral ROIs and used for correlational analyses.

374

375 **Task-related fMRI and behavioural data**

376 We used the Statistical Parametric Mapping (SPM) software package (SPM8; Wellcome Department of
377 Imaging Neuroscience, London, UK, <http://www.fil.ion.ucl.ac.uk>) for pre-processing and statistical analysis
378 of the functional MRI data. The first four volumes of a session (dummy images) were discarded from further
379 analysis. Whole-brain EPIs, including reversed-phase EPI, were recorded to facilitate the accurate
380 registration of the EPI data to the individual T1-weighted image. The EPI time series was motion corrected,
381 brain extracted and smoothed with a 1 mm two-dimensional Gaussian smoothing kernel (Fischl and Dale,
382 2000). We choose a small smoothing kernel to minimize the smearing of task-related somatosensory
383 processing in the postcentral gyrus into the precentral gyrus.

384 We specified a first-level general linear model to assess differences in brain activity between the movement
385 and rest blocks for each hand muscle. Two regressors-of-interest were defined for the blocks requiring
386 isometric abduction movements of the left index finger (engaging the FDI muscle) or little finger (engaging
387 the ADM muscle). To account for shifts in the onset of the hemodynamic response, temporal derivatives of
388 the resulting time courses, motion, respiration and cardiac cycle were included in the model as regressors-of-
389 no-interest (Friston et al., 1997; Smith et al., 2004). After model estimation, z-statistical images were
390 calculated for the resulting maps of the parameter estimates and a corrected statistical threshold of $p < 0.05$
391 was applied at the cluster level based on Gaussian random field theory (Worsley et al., 1996). The cluster
392 extent threshold was set to an uncorrected $p < 0.001$ (here corresponding to a Z-score of 3.2). For reporting,
393 the Z-statistical images were projected into Montreal Neurological Institute (MNI) space based on a
394 nonlinear registration of the T1-weighted structural MRI on the MNI152 template (using FSL FNIRT;
395 <http://fsl.fmrib.ox.ac.uk/fsl/slwiki>). In addition, average activation maps across subjects were rendered on the

396 FreeSurfer group template (figure 1) for visualization using the registration procedures as described in the
397 online FreeSurfer tutorial (<https://surfer.nmr.mgh.harvard.edu/fswiki/FsTutorial/FsFeatFreeSurfer>).

398 During the visually cued isometric finger abduction task, we extracted the mean interval between two
399 consecutive isometric contractions (i.e., inter-movement interval), its standard deviation (SD). Specifically,
400 the signal was thresholded at a level of 0.6 V and the findpeaks matlab function was used to identify peaks
401 with a minimum distance of 400 ms and a peak prominence of 1/3 of the maximum force value exerted by
402 the subject. As the movement onsets were quite steep, we found it reasonable to use these peaks to define
403 movement intervals. Importantly, the limited dynamic range of the force measurement setup caused the
404 exerted force to often go beyond the maximum, this meant that the force measurements were only of limited
405 practical use in this setting. Lastly, we calculated the coefficient of variation (CV) by dividing the SD with
406 the mean to quantify between-trial dispersion of movement timing. The CV of the inter-movement interval
407 indicates how well participants reproduced the one-per-second interval as signalled by the visual cue.

408

409 **Electric field simulations**

410 For each participant, we performed simulations of the electric fields that were generated in the right
411 precentral gyrus by the TMS pulse using SimNIBS software 2.0 (www.simnibs.org). A realistic head model
412 was automatically generated for each participant from the individual T1-weighted and T2-weighted MR
413 images as described elsewhere (Thielscher et al., 2015). Electric field simulations were calculated for the coil
414 position which elicited the highest mean MEP amplitude (i.e., the individual precentral motor hotspot) in left
415 FDI muscle and a stimulation intensity scaled to the individual RMT of FDI to clearly visualize the effect of
416 gyral anatomy on TMS-induced field strength. The TMS-related parameters to compute the E field strength
417 (i.e., coil location, stimulus intensity) were obtained before the main TMS mapping experiment, when we
418 conventionally determining the individual RMT of the FDI muscle by trial-and-error (Groppa et al., 2012).
419 Hence, the E-field calculations represent the maps that one normally would derive in standard TMS
420 experiments at the individual precentral motor hot spot. The vector potential of the MC-B35 coil was pre-
421 calculated using a coil model consisting of a superposition of 1248 magnetic dipoles, as described in
422 Thielscher and Kammer (Thielscher and Kammer, 2004). To obtain average electric fields across subjects,
423 the electric fields were interpolated in the middle of the segmented cortical grey matter, and transformed to

424 the FSAverage template (Fischl, 2012) for second-level group analyses. We then created a group map of the
425 electrical field distributions for the motor hotspot locations and statistically compared the TMS-induced
426 electrical field distributions in the right precentral hand knob between the M1_{HAND} and PMd group. Since the
427 rostral M1_{HAND} is confined to the posterior lip region of the precentral gyrus (Geyer et al., 1996), we
428 hypothesized that the M1_{HAND} group should display a higher electrical field magnitude in the posterior lip
429 region relative to the PMd group.

430

431 **Statistical group analyses**

432 All the statistical computations were performed using IBM SPSS Statistics software (Version 22 for
433 Windows, New York City, USA). Before applying parametric statistical tests, the normal distribution of all
434 variables was verified by means of a Kolmogorov and Smirnov test.

435 In a first set of analyses, we explored the structural, functional and |E| field properties of the rostral and
436 caudal part of the precentral motor hand knob. Individual estimates of myelination (derived from R1-
437 mapping), cortical thickness (derived from T1-weighted MRI scans), mean electric field strengths, and mean
438 task-related BOLD signal increase for index and little finger movements were extracted from the two
439 precentral ROIs in the right precentral hand knob, corresponding to the caudal Pre-CG and rostral Pre-CG.
440 For each variable, we computed separate paired t-tests to assess morpho-functional differences between the
441 two precentral ROIs. Finger movement (index vs little finger) was included as additional within-subject
442 factor in the ANOVA models analysing fMRI data and related performance measures.

443 A second set of analyses focused on the neurophysiological data recorded during sulcus-shape based TMS
444 mapping of the left FDI and ADM muscle. Our primary interest was to capture inter-individual differences in
445 cortico-muscular representation in the right precentral motor hand knob along the anterior-posterior axis. To
446 quantify inter-individual variation in rostro-caudal cortico-muscular representation, we derived a composite
447 measure for each participant that integrated the spatial (y-coordinate of precentral motor hot spot) and the
448 temporal dimension (corticomotor MEP latency at motor hot spot) of hot-spot rostrality. We reasoned that
449 the most robust way of quantifying functional rostrality of the corticomotor representation would be to derive
450 a composite measure that integrates both, the spatial and temporal dimension of functional rostrality. The
451 spatial dimension specifies how far the primary site of stimulation is away from the corticospinal output

452 neurons and the temporal dimension reflects how long does it take from the primary side to induce a
453 transsynaptic excitation of the corticospinal output neurons.

454 In each participant, we first took the shortest MEP latency that had been obtained at the motor hotspot for
455 both ADM and FDI muscles, and the corresponding y-coordinate of the respective muscle. We normalized
456 each measure by scaling it between 0 and 1, with 0 corresponding to the shortest latency and the most
457 posterior hotspot and 1 to the longest latency and most anterior hotspot. The two normalized variables were
458 then multiplied yielding a muscle- and subject-specific “hotspot rostrality index”. To test whether the spatial
459 and temporal dimensions of the hotspot rostrality index are related, we calculated the Pearson’s correlation
460 coefficient between the individual y-coordinate of the hot spot and the shortest MEP latency at motor hotspot
461 for the respective muscle.

462 The third set of analyses addressed the main question of this study and tested for function-structure
463 relationships in the right precentral motor hand knob. We hypothesized that inter-individual variations in
464 precentral myelin content would account for between-subject differences in precentral motor function (i.e.,
465 hot spot rostrality and task-related activation) and task performance (i.e., temporal synchronization of
466 repetitive finger movement). Using the mean R1-signal of the entire Pre-CG ROI as index of cortical
467 myelination, we calculated the Pearson’s correlation coefficient between the mean precentral R1-value and
468 individual functional read-outs such as the spatiotemporal rostrality index of the precentral motor hot spot,
469 mean task-related activation and the stability of the between-movement interval during the visually cued
470 movement synchronization task. Correlation analyses were conducted for each muscle (motor hotspot
471 rostrality) or finger (task-related activation and performance during the cued movement synchronization
472 task). Significance threshold was set at $p < 0.05$ and the Bonferroni procedure was used to correct for multiple
473 comparisons performed in each set of analyses. Data are given as mean (\pm SEM) if not otherwise specified.

474 We computed several follow-up analyses. We repeated the correlational analyses using only the mean MRI
475 signal from the rostral and caudal Pre-CG ROI to see whether linear structure-function relationships were
476 evenly expressed in the two ROIs. We also performed the same set of analyses using mean cortical thickness
477 rather than the mean R1-signal to exclude that the results were driven by differences in thickness of the
478 precentral hand knob. We also computed exploratory correlational analyses to assess the relationship

479 between spatiotemporal hotspot rostrality of the FDI and ADM hot spots and functional MRI-based and
480 behavioural read-outs.

481 To visualize the spatial expression of significant correlations at the voxel level within the right precentral
482 hand knob, we computed additional surface-based analyses within the precentral ROI on the FsAverage
483 template by using Freesurfer software. These analyses were performed vertex-wise, followed by cluster-wise
484 corrections for multiple comparisons based on the method suggested by Hagler and colleagues (Hagler et al.,
485 2006) (cluster-determining threshold: $p < 0.001$, cluster-wise correction $p < 0.05$). Age at the time of MRI and
486 sex were included in the model as nuisance variable. Finally, a separate surface between group analysis was
487 used to compare the spatial distribution difference of E-field between the two groups of participants
488 (posterior lip stimulation vs top of crown stimulation). Since we had a highly specific anatomical hypothesis
489 (posterior lip region), the explorative between-group analysis of electrical field distribution in precentral
490 gyrus applied a more liberal cluster extent threshold of $p < 0.01$.

491

492 **Results**

493 **Cortical myelination, thickness and curvature**

494 The structural properties of the right precentral hand knob were assessed with quantitative structural MRI,
495 using the mean R1-value of caudal and rostral part of the Pre-CG as index of regional myelination (see
496 methods section for details). The R1-value was only available in 20 of the 24 subjects, as the quantitative
497 MRI data of four subjects had to be excluded because of head movement related artefacts. The caudal part of
498 the Pre-CG showed higher mean R1 values than its rostral part (Caudal Pre-CG ROI: $796.48 \pm 8.51 \text{ ms}^{-1}$ vs
499 rostral Pre-CG ROI: $756.75 \pm 9.29 \text{ ms}^{-1}$, paired t-test: $t_{(19)} = 5.069$, $p < 0.001$, Fig. 2B). We also ran voxel-
500 wise analysis and surface rendering to visualize the regional expression of R1-values which showed that the
501 regional R1 signal gradually decreased along a caudal-to-rostral gradient in the precentral hand knob
502 (Fig.2B). To capture macrostructural features of the precentral motor hand knob, we derived cortical
503 thickness and curvature from the T1-weighted MRI images. On average, the cortex was thicker in the rostral
504 part of the precentral motor hand knob than in its caudal part (Caudal Pre-CG ROI: $2.51 \pm 0.04 \text{ mm}$ vs
505 rostral Pre-CG ROI: $2.73 \pm 0.03 \text{ mm}$, paired t-test: $t_{(23)} = -6.431$, $p < 0.001$, Fig. 2D). Cortical folding,
506 indexed by regional mean curvature was larger in the caudal part than in the rostral part of the precentral

507 motor hand knob (Caudal Pre-CG ROI: $0.02 \pm 0.01 \text{ mm}^{-1}$ vs rostral Pre-CG ROI: $-0.08 \pm 0.01 \text{ mm}^{-1}$, paired t-
508 test: $t_{(23)} = 42.368$, $p < 0.001$).

509

510 **Precentral corticomotor representations**

511 In each participant, the mean peak-to-peak MEP amplitude at each cortical stimulation site was used to
512 create two-dimensional maps of the corticomotor representations of the FDI and ADM muscle (Fig. 3A).
513 This enabled us to identify the precentral motor hotspot for each muscle, i.e. the stimulation site at which
514 mean MEP amplitude was largest. Mean MEP amplitude at motor hotspot was $1.11 (\pm 0.17) \text{ mV}$ for the FDI
515 muscle and $0.50 (\pm 0.08) \text{ mV}$ for the ADM muscle, reflecting the fact that MEP amplitudes were overall
516 larger for the FDI muscle. Since we mapped the spatial representation of MEP amplitudes along five parallel
517 lines in parallel to the curvature of the precentral gyrus, we were able to estimate the “rostrality” of the
518 individual hotspot along the anterior-posterior dimension of the precentral gyrus. In agreement with our
519 hypothesis, the position of individual motor hotspots along the rostro-caudal direction varied across
520 participants. Based on the rostrality of precentral hotspot location, we assigned participants to a “rostral
521 hotspot” group in which the hotspot located on one of the three anterior lines ($n= 14$) or to a “caudal hotspot”
522 group in which the hotspot located on one of the two posterior lines close to the central sulcus ($n= 10$). Table
523 1 summarizes mean group data for the entire group as well as for the rostral and caudal hotspot sub-group
524 separately. Groups were matched in terms of overall efficacy to excite the corticomotor output (table 1).
525 Mean MEP amplitudes at hotspot and cortical excitation thresholds for evoking a motor response did not
526 differ between the rostral and caudal hotspot sub-group for both muscles (FDI muscle: $t(22)= 14.461$, $p=$
527 0.434 ; ADM muscle: $t(22)= 21.611$, $p= 0.503$; unpaired t-test).

528 We extracted the stereotactic coordinates to systematically assess the topographical distribution of the motor
529 hotspots in the precentral motor hand knob. Using the stereotactic hotspot coordinates as dependent variable,
530 we computed a mixed-model ANOVA using group assignment as between-subject factor and *hand muscle*
531 (FDI vs ADM muscle) and *axis of stereotactic coordinate* (x-, y-, and z-direction) as within-subject factors.

532 The ANOVA validated our group assignment, showing an interaction between *coordinates* and *group*
533 ($F_{(2,44)}= 6.049$, $p=0.005$). Post-hoc analyses were performed to test for between-group differences of hotspot
534 locations along the x-, y-, and z-directions. The “rostral hotspot” and “caudal hotspot” groups only differed

535 with respect to their y-coordinates, corresponding to the sagittal (anterior-posterior) dimension in stereotactic
536 space. Mean y-coordinates of both muscles was -21.5 ± 1.3 in the “rostral hotspot” group and -14.1 ± 0.7 in
537 the “caudal hotspot” group ($t(22) = -7.382$; $p < 0.001$; Bonferroni-corrected t-test). The ANOVA also showed
538 an interaction between *coordinates* and *muscle* ($F_{(2,44)} = 8.299$, $p = 0.001$), confirming a significant difference
539 in precentral location between the FDI and ADM motor hotspots. Specifically, ADM muscle was located
540 more medially ($t(22) = 3.312$; $p = 0.005$; Bonferroni-corrected t-test) and superiorly ($t(22) = -2.598$; $p = 0.005$;
541 Bonferroni-corrected t-test) relative to the hotspot of the FDI muscle. This finding replicates our previous
542 sulcus-aligned mapping studies, using a single line of targets placed at the caudal border of the precentral
543 crown (Raffin et al., 2015; Dubbioso et al., 2017; Raffin and Siebner, 2018). Finally, ANOVA also revealed
544 main effects of the factors *group* ($F_{(1,22)} = 47.491$, $p < 0.001$) and *coordinates* ($F_{(2,44)} = 251.644$, $p < 0.001$).

545

546 **Spatiotemporal “rostrality” of precentral motor hotspot**

547 We hypothesized that the “spatial rostrality” of the motor hotspot scaled linearly with its “temporal
548 rostrality” resulting in longer cortico-to-motor conduction time. We therefore tested for a positive linear
549 relation between the antero-posterior coordinate (y) of the motor hotspot and the shortest MEP latency
550 evoked at the hotspot. We found that individual corticomotor latencies scaled positively with spatial
551 rostrality of individual motor hotspot locations in the precentral hand knob (Fig.3B). The more anterior
552 (rostral) the motor hotspot was located along the anterior-posterior (sagittal) direction, the longer was
553 corticomotor latency. Considering the data of all participants, we found a significant positive linear
554 relationship between y-coordinate of the motor hotspot and shortest MEP latency at hotspot, both for the FDI
555 muscle ($r = 0.697$, $p < 0.001$) and ADM muscle ($r = 0.555$, $p = 0.005$). No such relationship was found for the
556 medio-lateral x-coordinate (Fig.3B) and superior-inferior z-coordinate (FDI muscle: $r = 0.084$, $p = 0.697$;
557 ADM muscle: $r = 0.109$, $p = 0.614$). This association confirms our hypothesis that cortical precentral
558 excitation occurs functionally more “up-stream” to the cortico-motoneuronal neurons, when the preferential
559 target site is located more rostrally in the crown of the precentral hand knob.

560 Our sulcus-aligned TMS mapping procedure yielded a spatial (y-coordinate) and a temporal (MEP-latency)
561 rostrality measure of the individual TMS target site in the gyral crown of the precentral hand knob.
562 Considering both, the spatial and temporal rostrality dimensions, we computed a “spatiotemporal rostrality

563 index” of the TMS hotspot (see Methods section for details). This spatiotemporal rostrality index reflects
564 how much TMS preferentially excites cortical neurons in the caudal PMd or M1_{HAND}. At the individual level,
565 the spatiotemporal rostrality index of the FDI and ADM muscle showed a positive linear relationship ($r=$
566 0.819, $p<0.001$), showing that hotspot rostrality of the two hand muscles was consistently expressed at the
567 single-subject level.

568

569 **Precentral myelination scales with spatiotemporal rostrality of precentral motor hotspot**

570 The regional myelination of the precentral hand knob as indexed by the mean R1-value showed a significant
571 positive linear relationship with individual spatiotemporal rostrality index. The higher the mean R1-signal in
572 the right precentral hand knob, the higher was the rostrality index of the precentral motor hot spot (Fig.4).
573 This positive relationship was found for the FDI hotspot ($r= 0.699$, $p<0.001$, Fig.4A) and ADM hotspot ($r=$
574 0.637, $p= 0.003$, Fig.4C). Surface-based correlation analyses pinpointed a rostro-lateral cluster in the anterior
575 lip region of the precentral crown where regional R1-values correlated most strongly with the individual
576 spatiotemporal rostrality index with peak correlation at $x, y, z = 32.6, -11.3, 53.6$ for the FDI muscle
577 (Fig.4B) and at $x, y, z = 34.8, -11.6, 59.2$ for ADM muscle (Fig.4D). A second cluster was located dorsal and
578 medially in the posterior lip region of the precentral gyrus. Correlation peaked at $x, y, z = 26.6, -22.7, 51.8$
579 for the FDI muscle and at $x, y, z = 29.3, -21.8, 58.7$ for the ADM muscle. Both hand muscles expressed a
580 positive linear relationship in the caudal Pre-CG (FDI muscle: $r= 0.720$, $p< 0.001$; ADM muscle: $r= 0.591$,
581 $p= 0.006$) and rostral Pre-CG (FDI muscle: $r= 0.625$, $p= 0.003$; ADM muscle: $r= 0.571$, $p= 0.007$).

582 At the individual level, regional thickness of the right precentral gyrus did not predict spatiotemporal
583 rostrality of the precentral motor hotspot. No significant correlation was found between cortical thickness
584 and the individual rostrality index for both muscles (FDI muscle: $r= -0.230$, $p= 0.280$; ADM muscle: $r= -$
585 0.277, $p= 0.190$). There was also no significant correlation between mean curvature of the right precentral
586 gyrus and the rostrality index for both muscles (FDI muscle: $r= 0.146$, $p= 0.495$; ADM muscle: $r= -0.021$, $p=$
587 0.924). Together, these negative results show that the association between regional myelination and
588 spatiotemporal rostrality of the precentral hotspot was not driven by differences in cortical volume and mean
589 curvature.

590

591 Myelination of the precentral hand knob has functional and behavioural correlates

592 Our multimodal mapping approach revealed a link between cortical myelin content and functional cortico-
593 motor representations in the precentral motor hand knob and timing proficiency during stereotyped finger
594 movements. While the right precentral motor hand knob was consistently activated when participants
595 performed visually cued finger movements at a repetition rate of 1Hz, the rostral part of the precentral Mean
596 task-related BOLD increase was stronger in the caudal Pre-CG ROI (1.6 ± 0.13) compared to the rostral Pre-
597 CG ROI (1.26 ± 0.09), paired t-test: $t_{(23)} = 3.401$, $p = 0.002$ (Fig.2C). We tested whether the degree of
598 precentral myelination predicts the magnitude of task-related regional activation and task performance. We
599 found a positive linear correlation between the mean cortical R1 signal within the precentral motor hand
600 knob and the magnitude of cortical activation during the visuo-motor synchronization task (Fig.5). This
601 positive relationship was found regardless of whether the task was carried out with the index ($r = 0.659$, $p =$
602 0.002 , Fig.5A) or little finger ($r = 0.748$, $p < 0.001$, Fig.5C). Surface-based correlation analyses located the
603 regional expression of this relationship to a rostro-lateral cluster in the anterior lip region of the precentral
604 crown where regional R1-values correlated most strongly with regional task-related activation during
605 repetitive movements with the index finger (peak correlation at $x, y, z = 28.3, -14.4, 63.1$; Fig.5B) or little
606 finger ($x, y, z = 27.6, -14.1, 65.2$; Fig.5D). The linear relationship between cortical myelination and task-
607 related activation was expressed in the rostral precentral ROI (FDI muscle: $r = 0.655$, $p = 0.002$; ADM
608 muscle: $r = 0.554$, $p = 0.011$), but also in the caudal precentral ROI for the ADM muscle ($r = 0.591$, $p = 0.006$)
609 and trend-wise for the FDI muscle ($r = 0.404$, $p = 0.078$).

610 Precentral myelination did not only predict task-related BOLD signal changes in the precentral motor hand
611 knob, but also the temporal reliability of movement repetition in the visuomotor synchronization task (Fig.6)
612 We found that participant more precisely synchronized their finger movements to the external pace, the
613 higher the precentral myelin content. There was a significant negative linear relation between precentral
614 cortical myelination, as indexed by regional R1-value, and the mean CV of movement repetition rate for both
615 fingers, index finger: $r = -0.619$, $p = 0.004$ and little finger: $r = -0.684$, $p < 0.001$ (Fig. 6A, C). This indicates
616 that individuals with a higher degree of cortical myelination of the precentral gyrus showed a more regular
617 timing of repetitive finger movements with less inter-trial variation of the between-movement interval.
618 Surface-rendered maps of this relationship at voxel levels yielded several clusters which were mainly

619 located, but not limited, in the precentral crown (Fig.6B, D). Follow-up analyses based on the mean R1-
620 signal from the two Pre-CG ROIs revealed that the myelin content in the rostral (index finger: $r = -0.601$, $p =$
621 0.004 ; little finger: $r = -0.662$, $p = 0.001$) and caudal part of the motor hand knob (index finger: $r = -0.590$, $p =$
622 0.006 ; little finger: $r = -0.626$, $p = 0.003$) scaled negatively with the mean CV of movement repetition rate for
623 both fingers.

624 We also performed exploratory analyses in which we tested for linear relationships between hotspot
625 rostrality and functional motor read-outs (FDI muscle: $r = 0.450$, $p = 0.031$; ADM muscle: $r = 0.525$, $p =$
626 0.008). Like for the mean R1-signal in precentral gyrus, we found that inter-individual variations in BOLD-
627 signal change and movement repetition rate also scaled linearly with individual hotspot rostrality, showing
628 that this functional TMS readout also reflects inter-individual differences in cortical motor function at the
629 level of regional neural activity and timing performance (FDI muscle: $r = -0.617$, $p = 0.0013$; ADM muscle:
630 $r = -0.619$, $p = 0.0013$).

631

632 **Hotspot location is related to induced electrical field magnitude in precentral gyrus**

633 Since all participants underwent structural T1-weighted and T2-weighted MRI scans, we were able to
634 simulate the electric fields that were generated in the right precentral gyrus by the TMS pulse at the
635 individual precentral hotspot as determined in the preparatory TMS session. We first created a group map of
636 the electrical field distributions for the motor hotspot locations. Electric field strength was high in the
637 precentral crown and weak in the sulcal parts of the precentral gyrus (Fig. 2E). We statistically compared the
638 TMS-induced electrical field distributions in the right precentral hand knob between the group with a rostral
639 or a caudal hotspot location in the main experiment (Fig. 7). The colour-coded surface rendered maps of the
640 regionally induced electrical field confirmed that the average of electric field strength was maximal in the
641 precentral crown corresponding to the precentral hand knob with additional local peaks with lower intensity
642 in neighbouring gyral crowns (Fig.7A,B). Although the spatial distribution of the TMS-induced electrical
643 fields was similar in the right precentral hand knob, between-group comparison revealed higher electrical
644 field magnitudes in the posterior lip region in the group having a more caudal hotspot location in the shape-
645 based TMS mapping experiment (Fig.7). The between-group difference in electrical field magnitude peaked
646 at the x-,y-,z-coordinates 34, -20, 65, corresponding to the posterior lip region of the precentral gyrus. The

647 group with a more rostral motor hotspot did not display any clusters in the precentral gyrus where the
648 induced electrical field was higher than in subjects with a more caudal hotspot location. Hence, electrical
649 field strength did not differ between groups in the anterior lip region of the precentral gyrus. In a follow-up
650 analysis, we tested whether the individual E-field strength in precentral gyrus scales would scale with
651 precentral cortical myelin content. We found no cluster in the precentral gyrus showing a significant linear
652 relationship between individual E-field strength and cortical myelin content.

653 **Discussion**

654 In healthy human volunteers, we probed the regional structure and function of the right precentral motor
655 hand knob with TMS, structural and functional MRI. Our multimodal brain mapping approach revealed a
656 link between cortical myelin content, functional cortico-motor representations, and dexterous motor control.
657 A higher myelin content of the precentral motor hand knob was associated with more rostral corticomotor
658 presentations as revealed by shape-informed TMS mapping, with stronger task-related activation during task-
659 based fMRI, and a higher precision of movement timing during a visuo-motor synchronization task.

660

661 *Relationship between precentral myelin content and rostrality of corticomotor muscle presentations*

662 The spatial location of the motor hotspot, defined as the optimal scalp position where TMS evokes a
663 contralateral motor response, varied across individuals along an anterior-posterior axis. In contrast to
664 standard grid-based mapping, our sulcus-aligned mapping procedure secured that TMS at each stimulation
665 site produced a consistent current direction in the most strongly stimulated part of the precentral hand knob
666 regardless of the individual folding pattern. Extending previous work, we found that a more rostral hotspot
667 location in the precentral crown was associated with a longer corticomotor MEP latency. In individuals, in
668 whom the motor hot spot was spatially more distant from the central sulcus, stimulation also occurred
669 functionally more upstream from the corticospinal motoneurons, resulting in longer latencies. In other
670 words, “spatial” rostrality of the individual motor hotspot was mirrored by a “temporal” or “functional”
671 rostrality of the motor hotspot. MRI mapping of the R1 signal revealed that the spatiotemporal “hotspot
672 rostrality” had a structural correlate in the precentral hand knob. The degree of precentral myelination,
673 reflected by the mean regional R1 signal, but not cortical thickness scaled with inter-individual differences in
674 spatiotemporal “hotspot rostrality”.

675

676 ***TMS of the motor hand knob is spatially biased towards the superficial crown-lip region***

677 The human M1-HAND consists of a posterior (or caudal) region which is located in the depth of the anterior
678 sulcal wall (referred to as BA4p) and an anterior (or rostral) region (referred to as BA4a) which is located
679 more superficially in the anterior wall and may expand into the superficial crown-lip region (Geyer et al.,
680 1996,2000). Retrograde tracing studies in the macaque monkey identified the caudal portion of M1 in the
681 anterior bank of the central sulcus as the main precentral source of cortico-motoneuronal pyramidal output
682 neurons (Rathelot and Strick, 2006, 2009). The number of fast-conducting corticospinal pyramidal output
683 neurons with direct synaptic connections to the cervical motoneurons are mainly found in the caudal “new”
684 portion of the M1-HAND corresponding to area BA4p in humans (Rathelot and Strick, 2006, 2009). Since
685 the vast majority of fast-conducting corticospinal pyramidal output neurons originate from the caudal M1-
686 HAND in the depth of the central sulcus, these neurons but also the axons of other interneurons and
687 pyramidal cells in caudal M1-HAND (BA4p) are “out of reach” for the TMS-induced electrical field which
688 primarily targets the superficial crown-lip region in the precentral gyrus. We therefore argue that cortical
689 regions that are located more superficially and are functionally more “upstream” such as the rostral M1-
690 HAND (BA4a) and the caudal part of PMd are the primarily excited cortical areas, when TMS is applied to
691 the motor hot spot. The primary stimulation of superficial precentral areas then causes a transsynaptic
692 (indirect) excitation of fast-conducting corticospinal output neurons via cortico-cortical axonal projections
693 from anterior M1-HAND and the caudal part of PMd to the posterior M1-HAND (Siebner, 2020).

694 A recent biophysical modelling study identified axonal terminations in the crown-lip region of the precentral
695 gyrus, that are aligned to the locally induced e-field direction, as primary target structures for TMS-induced
696 neuronal excitation (Aberra et al., 2020). Efficient excitation of axonal terminations within the precentral
697 crown-lip region will lead to transsynaptic excitation of other cortical neurons in this area (i.e., axonal-
698 termination hypothesis). The highly synchronized neuronal activity in the stimulated crown-lip region may
699 then spread to deeper parts of the precentral cortex (especially the caudal M1-HAND) in the sulcal wall via
700 cortico-cortical axonal fibers. Alternatively, it is possible that the induced electrical field primarily stimulates
701 the bends of juxtacortical cortico-cortical axons that originate in the precentral crown and project into the
702 depth of the sulcus where the bulk of the fast-conducting corticospinal motoneurons are located (i.e., axonal-

703 bend hypothesis). Electric field modelling suggests that the field strength in juxta-cortical white matter of the
704 precentral crown is indeed higher than the field strength in the overlying gray matter (Thielscher et al.,
705 2011), and axonal bends have been identified as putative stimulation sites based on morphologically
706 simplified neural models (Salvador et al., 2011).

707

708 *Direction-specific target engagement of axonal structures in the precentral crown*

709 We used biphasic TMS pulses for shaped-informed TMS mapping as in our previous studies (Raffin et al.,
710 2015; Dubbioso et al., 2017; Raffin and Siebner, 2018). The biphasic pulse produced two neurobiologically
711 relevant currents in the precentral gyrus: the first phase of the biphasic pulse produced an Anterior-to-
712 Posterior (A-P) directed current, while the second phase caused a current with a Posterior-to-Anterior (P-A)
713 direction. The second P-A component is neurobiologically most effective given the longer duration and
714 larger area-under-the-curve, but the first A-P component may also induce action potentials and contribute to
715 the MEP. The direction-dependent effects of the A-P and P-A components of the biphasic pulse may
716 determine the anterior-posterior hot spot location. In their modelling study, Aberra et al. (2020) showed that
717 a monophasic TMS pulse producing an A-P directed current in the precentral gyrus resulted in an anterior
718 shift of activation of axon terminals of pyramidal neurons in layer two or five compared to a monophasic
719 TMS pulse causing a current in the opposite (P-A) direction. Interestingly, this pattern also emerged albeit to
720 a lesser extent, when simulating the precentral crown with a biphasic pulse configuration (Aberra et al.,
721 2020). This implies that a P-A directed current will result in lower thresholds for efficient axonal
722 depolarization in the posterior lip region, while an A-P directed current will result in lower excitation
723 thresholds in the anterior lip region of the crown. The biophysical properties of biphasic TMS may account
724 for the present results. The A-P component of the TMS pulse may have been more relevant for overall
725 stimulation of axonal structures in the precentral crown in individuals with a more anterior precentral motor
726 hotspot location: In these individuals, the A-P current may have been more effective to induce
727 suprathreshold depolarization of axonal terminations in the anterior lip region. Conversely, the depolarizing
728 effects of the P-A current may be more prevalent in individuals with a more posterior motor hotspot location.
729 In these individuals, a preponderant excitation of axonal terminations in the posterior lip region may have
730 shifted the precentral motor hotspot posteriorly. This explanation is corroborated by the simulations of the
731 TMS-induced electrical field at the hot spot location. Here, TMS induced a stronger electrical field in the

732 posterior lip of the precentral crown only in individuals in whom sulcus-shaped TMS mapping revealed a
733 caudal posterior precentral motor hotspot.

734 In addition to intracortical excitation of axon terminals, a biphasic TMS pulse may effectively depolarize
735 longer-range juxtacortical axons at their bends in the subcortical white matter within the precentral crown-lip
736 region. Since the depolarizing effect of the electrical field on the axonal bend depends on its orientation
737 relative to the e-field, the A-P and P-A directed currents may result in spatially distinct hotspots. The A-P
738 directed current preferentially stimulates axonal bends in more anterior (rostral) locations within the
739 precentral crown, whereas the P-A directed current may preferentially stimulate axonal bends in more
740 posterior (caudal) locations in the precentral crown. The capability to excite these axon bends may differ
741 across individuals and thus, contribute to inter-individual variations in motor hotspot location.

742

743 ***Positive linear relationship between spatial and temporal hot spot rostrality***

744 In our study, participants with a more rostral hotspot had longer corticomotor latencies than those with a
745 more caudal hot spot location. The inter-individual variation in corticomotor latencies may be caused by the
746 inter-individual variation in preferential A-P stimulation in the precentral crown. According to the axonal-
747 termination hypothesis, a preferential stimulation of axonal terminations in the anterior lip region (A-P
748 current) or posterior lip region (P-A current) of the precentral crown will alter the cortico-cortical conduction
749 time from the precentral crown to the caudal M1-HAND (BA4p area) in the depth of the central sulcus. This
750 explanation is in good agreement with previous TMS studies on the impact of a current reversal for
751 monophasic pulse configurations: Reversing the current flow from PA to AP in the precentral crown also
752 results in longer corticomotor latencies and higher corticomotor thresholds (Hamada et al., 2013) and
753 stronger susceptibility to variations in pulse length (D'Ostilio et al., 2016). Furthermore, MEP-latency after
754 AP-TMS was found to correlate with functional connectivity between M1 and a network involving cortical
755 premotor areas (Volz et al., 2015).

756 The axonal-bend hypothesis may also explain the observed variation in corticomotor latency. The folding of
757 the cortex at the gyral crown alters the curvature of axonal bends in the juxta-cortical part of the anterior and
758 posterior lip region which renders these spatially segregated segments of the same axons more or less
759 susceptible to the anterior-posterior phase of the biphasic TMS pulse. Accordingly, the A-P and P-A current

760 components of the biphasic pulse may stimulate the same juxta-cortical cortico-cortical axons at more
761 anterior or posterior positions in the precentral crown. In humans, TMS activates neural elements having
762 time constants determined from strength–duration curves of roughly 200 μ s (Barker et al., 1991; Peterchev et
763 al., 2013; D’Ostilio et al., 2016) with conduction times comparable to peripheral motor axons. A very
764 conservative estimate would be that these axons have conduction speed of around 10 m/s (West and
765 Wolstencroft, 1983; Firmin et al., 2014). In this case, the observed MEP latency differences would
766 correspond to a travelled distance of >12 mm which is in the range of the observed variations of the hotspot
767 in caudal-rostral direction. For a slightly less conservative estimate of conduction speeds of 20 m/s or more,
768 the observed MEP latency differences are too long to be explained merely by the stimulation of two positions
769 of the same axons anymore, but rather favours the targeting of different neural populations. Finally, the axon
770 diameter distribution of cortico-cortical projection fibers within the precentral gyrus may have contributed to
771 the between-subject variations in corticomotor latency (Liewald et al., 2014). The larger the cortico-cortical
772 axons and the thicker their myelin sheets, the faster the signal transmission from the primary site of
773 stimulation in the precentral crown to the fast-conducting corticospinal output neurons originating from the
774 caudal M1-HAND (BA4p area) in the depth of the central sulcus.

775 ***Positive linear relationship between hotspot rostrality and precentral myelination***

776 Our results establish a link between the myelination of the precentral hand knob and motor hot spot location,
777 showing that the cortical myelin content scaled with individual motor hotspot rostrality. The axonal-
778 termination hypothesis of TMS-induced cortex stimulation can account for this positive relationship.
779 Stronger myelination of axons may lower the excitation threshold of axonal terminals in the anterior and
780 posterior crown-lip region of the precentral gyrus to fire action potentials in response to TMS. This may be
781 particularly relevant for the efficacy of the A-P component of the biphasic pulse which is less efficient than
782 the P-A component. If axon terminations are more myelinated in the anterior lip region of the central gyrus,
783 they will become more susceptible to the depolarizing effect of the A-P directed current. The A-P directed
784 current will contribute more to the overall stimulation of axonal terminations in the precentral crown and
785 shift the motor hotspot location to a more anterior location. Conversely, the motor hotspot will be located
786 more caudally if the P-A component makes the strongest contribution to overall axonal depolarization in the
787 precentral crown.

788 The axonal-bend hypothesis of TMS-induced cortex stimulation can also account for the positive relationship
789 between hotspot rostrality and the degree of precentral myelination. If juxtacortical axonal bends in the
790 anterior lip region are more strongly myelinated, they may be more easily depolarized by the A-P directed
791 current. A relatively stronger contribution of the A-P directed current to the overall excitation of axonal
792 bends in the precentral crown will result in an anterior shift of the motor hotspot.

793

794 *A macro-anatomical perspective on spatiotemporal hotspot variability*

795 Do the inter-individual differences in spatiotemporal hotspot rostrality indicate that TMS preferentially
796 excites cytoarchitectonically different cortex regions? The rostral M1-HAND (BA4a) and caudal PMd in
797 the precentral crown-lip regions are the primary target regions, when TMS is applied at the precentral motor
798 hot spot (Abera et al., 2020). The border between rostral M1-HAND and caudal PMd is not sharply
799 demarcated but smooth and the transition may vary considerable along the anterior-posterior axis in the
800 precentral gyrus (Geyer et al. 1996, 2000). In some individuals, the transition zone between M1-HAND and
801 PMd extends to the precentral crown-lip region, making the superficial part of the rostral M1-HAND a
802 primary target for TMS, in individuals with a caudal motor hot spot location. Therefore, one should be
803 cautious to conclude that in individuals with an anterior or posterior precentral hot spot, TMS preferentially
804 stimulates more rostral or caudal parts of PMd, respectively. It is also possible that TMS preferentially
805 stimulates the most anterior part of the rostral M1-HAND in individuals with a posterior precentral motor
806 hotspot.

807 In macaque monkeys, intracortical electrical stimulation revealed that both, the rostral (old) and caudal
808 (new) part of M1 send slowly conducting mono-synaptic corticospinal projections to the cervical
809 motoneurons, while only the caudal (new) M1 hosted pyramidal cells with fast monosynaptic corticospinal
810 projections to the cervical spinal motoneurons (Witham et al., 2016). In persons with a posterior precentral
811 hotspot, the slowly conducting mono-synaptic corticospinal projections to the cervical motoneurons may be
812 readily stimulated by TMS via excitation of local axonal terminals, if the rostral M1-HAND extends
813 rostrally into the posterior crown-lip region.

814

815 *Linking precentral myelination and motor function*

816 Regional myelination showed a positive linear relationship with motor activation in the precentral hand knob
817 during task-based MRI in the anterior lip region of the precentral crown. The stronger task-related
818 engagement of the right caudal PMd in individuals with a higher precentral myelin content is in good
819 agreement with previous work showing that the PMd plays a prominent role in visuomotor integration
820 (Jäncke et al., 2000; Sugiura et al., 2001; Cerasa et al., 2005; Chouinard and Paus, 2006; Witt et al., 2008;
821 Hardwick et al., 2015). We also identified several clusters in the rostral and caudal part of the precentral
822 motor hand knob where a higher cortical myelin content was associated with a higher degree of temporal
823 regularity during the finger tapping task. Our motor task probed temporal aspects of dexterous motor control,
824 because participants had to match the timing of tapping to the regular one-hertz pace given by an external
825 cue. Individuals with a higher precentral myelin signal were better at minimizing inter-trial variations
826 between consecutive movements. We therefore argue that a higher degree of myelination of the precentral
827 gyrus enabled a more precise synchronization of finger tapping with the regular pace provided by the visual
828 cue.

829 How does cortical myelination support the integration of neuronal activity within functional brain networks?
830 Structural MRI studies have linked cortical myelination to intrinsic functional connectivity (Huntenburg et
831 al., 2017) and task-related functional activity in unimodal cortical areas, including the visual (Sánchez-
832 Panchuelo et al., 2012; Sereno et al., 2013), auditory (Dick et al., 2012; Kim and Knösche, 2016), and
833 sensorimotor cortex (Glasser et al., 2016; Kuehn et al., 2017). Axonal myelination enables fast signal
834 propagation and synchronizes neural activity and determine properties of neuronal activity subserving
835 temporal coding, such as spike latency and inter-spike interval (Seidl et al., 2010; Pajevic et al., 2014; Ford
836 et al., 2015; Timmler and Simons, 2019). Our results lend further support to the notion that a high degree of
837 myelination in adult neocortex is critical to fast and temporally precise, regional neuronal processing,
838 suggesting that a high degree of precentral myelin content enables higher temporal precision during
839 dexterous hand use.

840

841 *Conclusion*

842 We provide first-time evidence for behaviourally relevant, structural and functional phenotypic variation in
843 the crown of the human precentral motor hand knob. Linking variations in regional brain structure and

844 function, regional excitability and dexterity, our results corroborate the functional relevance of cortical
845 myelin for cortical function and related behaviour.

846 Our results are also of relevance to the research community that uses TMS of the human $M1_{HAND}$ to study
847 motor cortex plasticity. Defining the individual precentral motor hotspot location is the standard method for
848 spatial targeting of human $M1_{HAND}$ (Groppa et al., 2012; Rossini et al., 2015). Our work questions the
849 assumption that hotspot-based targeting can secure a comparable stimulation of the precentral motor hand
850 knob across subjects. In recent years, it has been emphasized that the plasticity-induced effects of repetitive
851 TMS targeting $M1_{HAND}$ suffers from substantial inter-individual variability (López-Alonso et al., 2014;
852 Ziemann and Siebner, 2015). Inter-individual differences in motor hotspot rostrality may constitute a major
853 contributing factor to inter-individual differences in the after-effects on corticomotor excitability. Since
854 inter-individual differences in hotspot rostrality are associated with different microstructural properties in
855 terms of cortical myelination, it is possible that individuals with a more rostral or caudal motor hotspot may
856 express different forms of precentral motor plasticity.

857

858

859

860

861

862

863 **References**

864 Aberra AS, Wang B, Grill WM, Peterchev A V. (2020) Simulation of transcranial magnetic stimulation in
865 head model with morphologically-realistic cortical neurons. *Brain Stimul* 13:175–189.

866 Ahdab R, Ayache SS, Brugières P, Farhat WH, Lefaucheur JP (2016) The Hand Motor Hotspot is not

867 Always Located in the Hand Knob: A Neuronavigated Transcranial Magnetic Stimulation Study. *Brain*
868 *Topogr* 29:590–597.

869 Ahdab R, Ayache SS, Farhat WH, Mylius V, Schmidt S, Brugières P, Lefaucheur JP (2014) Reappraisal of

- 870 the anatomical landmarks of motor and premotor cortical regions for image-guided brain navigation in
871 TMS practice. *Hum Brain Mapp* 35:2435–2447.
- 872 Annese J, Pitiot A, Dinov ID, Toga AW (2004) A myelo-architectonic method for the structural
873 classification of cortical areas. *Neuroimage* 21:15–26.
- 874 Awiszus F (2003) Chapter 2 TMS and threshold hunting. Elsevier B.V.
- 875 Barker AT, Garnham CW, Freeston IL (1991) Magnetic nerve stimulation: the effect of waveform on
876 efficiency, determination of neural membrane time constants and the measurement of stimulator output.
877 *Electroencephalogr Clin Neurophysiol Suppl* 43:227–237.
- 878 Barker AT, Jalinos R, Freeston IL (1985) Non-invasive magnetic stimulation of human motor cortex.
879 *Lancet* 1:1106–1107.
- 880 Bungert A, Antunes A, Espenhahn S, Thielscher A (2017) Where does TMS Stimulate the Motor Cortex?
881 Combining Electrophysiological Measurements and Realistic Field Estimates to Reveal the Affected
882 Cortex Position. *Cereb Cortex* 27:5083–5094.
- 883 Cerasa A, Hagberg GE, Bianciardi M, Sabatini U (2005) Visually cued motor synchronization: Modulation
884 of fMRI activation patterns by baseline condition. *Neurosci Lett* 373:32–37.
- 885 Chen R, Cros D, Curra A, Di Lazzaro V, Lefaucheur JP, Magistris MR, Mills K, Rösler KM, Triggs WJ,
886 Ugawa Y, Ziemann U (2008) The clinical diagnostic utility of transcranial magnetic stimulation:
887 Report of an IFCN committee. *Clin Neurophysiol* 119:504–532.
- 888 Chouinard PA, Paus T (2006) The Primary Motor and Premotor Areas of the Human Cerebral Cortex.
889 *Neurosci* 12:143–152.
- 890 D’Ostilio K, Goetz SM, Hannah R, Ciocca M, Chieffo R, Chen JCA, Peterchev A V., Rothwell JC (2016)
891 Effect of coil orientation on strength-duration time constant and I-wave activation with controllable
892 pulse parameter transcranial magnetic stimulation. *Clin Neurophysiol* 127:675–683.
- 893 Dick F, Tierney AT, Lutti A, Josephs O, Sereno MI, Weiskopf N (2012) In vivo functional and
894 myeloarchitectonic mapping of human primary auditory areas. *J Neurosci* 32:16095–16105.
- 895 Diekhoff S, Uludağ K, Sparing R, Tittgemeyer M, Cavuşoğlu M, Von Cramon DY, Grefkes C (2011)
896 Functional localization in the human brain: Gradient-echo, spin-echo, and arterial spin-labeling fMRI
897 compared with neuronavigated TMS. *Hum Brain Mapp* 32:341–357.

- 898 Dubbioso R, Raffin E, Karabanov A, Thielscher A, Siebner HR (2017) Centre-surround organization of fast
899 sensorimotor integration in human motor hand area. *Neuroimage* 158:37–47.
- 900 Dum RP, Strick PL (2005) Frontal Lobe Inputs to the Digit Representations of the Motor Areas on the
901 Lateral Surface of the Hemisphere. *J Neurosci* 25:1375–1386.
- 902 Elston GN, Rockland KS (2002) The pyramidal cell of the sensorimotor cortex of the macaque monkey:
903 Phenotypic variation. *Cereb Cortex* 12:1071–1078.
- 904 Firmin L, Field P, Maier MA, Kraskov A, Kirkwood PA, Nakajima K, Lemon RN, Glickstein M (2014)
905 Axon diameters and conduction velocities in the macaque pyramidal tract. *J Neurophysiol* 112:1229–
906 1240.
- 907 Fischl B (2012) FreeSurfer. *Neuroimage* 62:774–781.
- 908 Fischl B, Dale AM (2000) Measuring the thickness of the human cerebral cortex from magnetic resonance
909 images. *Proc Natl Acad Sci* 97:11050–11055.
- 910 Ford MC, Alexandrova O, Cossell L, Stange-Marten A, Sinclair J, Kopp-Scheinpflug C, Pecka M, Attwell
911 D, Grothe B (2015) Tuning of Ranvier node and internode properties in myelinated axons to adjust
912 action potential timing. *Nat Commun* 6:8073.
- 913 Friston KJ, Buechel C, Fink GR, Morris J, Rolls E, Dolan RJ (1997) Psychophysiological and modulatory
914 interactions in neuroimaging. *Neuroimage* 6:218–229.
- 915 Geyer S, Ledberg A, Schleicher A, Kinomura S, Schormann T, Burgel U, Klingberg T, Larsson J, Zilles K,
916 Roland PE (1996) Two different areas within the primary motor cortex of man. *Nature* 382:805–807.
- 917 Geyer S, Matelli M, Luppino G, Zilles K (2000) Functional neuroanatomy of the primate isocortical motor
918 system. *Anat Embryol (Berl)* 202:443–474.
- 919 Glasser MF, Coalson TS, Robinson EC, Hacker CD, Harwell J, Yacoub E, Ugurbil K, Andersson J,
920 Beckmann CF, Jenkinson M, Smith SM, Van Essen DC (2016) A multi-modal parcellation of human
921 cerebral cortex. *Nature* 536:171–178.
- 922 Glasser MF, van Essen DC (2011) Mapping human cortical areas in vivo based on myelin content as
923 revealed by T1- and T2-weighted MRI. *J Neurosci* 31:11597–11616.
- 924 Groppa S, Oliviero A, Eisen A, Quartarone A, Cohen LG, Mall V, Kaelin-Lang A, Mima T, Rossi S,
925 Thickbroom GW, Rossini PM, Ziemann U, Valls-Solé J, Siebner HR (2012) A practical guide to

- 926 diagnostic transcranial magnetic stimulation: Report of an IFCN committee. *Clin Neurophysiol*
927 123:858–882.
- 928 Hagler DJ, Saygin AP, Sereno MI (2006) Smoothing and cluster thresholding for cortical surface-based
929 group analysis of fMRI data. *Neuroimage* 33:1093–1103.
- 930 Hamada M, Murase N, Hasan A, Balaratnam M, Rothwell JC (2013) The role of interneuron networks in
931 driving human motor cortical plasticity. *Cereb Cortex* 23:1593–1605.
- 932 Hardwick RM, Lesage E, Eickhoff CR, Clos M, Fox P, Eickhoff SB (2015) Multimodal connectivity of
933 motor learning-related dorsal premotor cortex. *Neuroimage* 123:114–128.
- 934 Helms G, Dathe H, Dechent P (2008) Quantitative FLASH MRI at 3T using a rational approximation of the
935 Ernst equation. *Magn Reson Med* 59:667–672.
- 936 Huntenburg JM, Bazin PL, Goulas A, Tardif CL, Villringer A, Margulies DS (2017) A Systematic
937 Relationship Between Functional Connectivity and Intracortical Myelin in the Human Cerebral Cortex.
938 *Cereb Cortex* 27:981–997.
- 939 Jäncke L, Loose R, Lutz K, Specht K, Shah NJ (2000) Cortical activations during paced finger-tapping
940 applying visual and auditory pacing stimuli. *Cogn Brain Res* 10:51–66.
- 941 Kammer T, Beck S, Erb M, Grodd W (2001) The influence of current direction on phosphene thresholds
942 evoked by transcranial magnetic stimulation. *Clin Neurophysiol* 112:2015–2021.
- 943 Kim SG, Knösche TR (2016) Intracortical myelination in musicians with absolute pitch: Quantitative
944 morphometry using 7-T MRI. *Hum Brain Mapp* 37:3486–3501.
- 945 Kuehn E, Dinse J, Jakobsen E, Long X, Schäfer A, Bazin PL, Villringer A, Sereno MI, Margulies DS (2017)
946 Body Topography Parcellates Human Sensory and Motor Cortex. *Cereb Cortex* 27:3790–3805.
- 947 Lang N, Harms J, Weyh T, Lemon RN, Paulus W, Rothwell JC, Siebner HR (2006) Stimulus intensity and
948 coil characteristics influence the efficacy of rTMS to suppress cortical excitability. *Clin Neurophysiol*
949 117:2292–2301.
- 950 Lemon R (2019) Recent advances in our understanding of the primate corticospinal system. *F1000Research*
951 8:F1000 Faculty Rev-274.
- 952 Lemon RN (2008) Descending Pathways in Motor Control. *Annu Rev Neurosci* 31:195–218.
- 953 Liewald D, Miller R, Logothetis N, Wagner HJ, Schüz A (2014) Distribution of axon diameters in cortical

- 954 white matter: an electron-microscopic study on three human brains and a macaque. *Biol Cybern*
955 108:541–557.
- 956 López-Alonso V, Cheeran B, Río-Rodríguez D, Fernández-Del-Olmo M (2014) Inter-individual variability
957 in response to non-invasive brain stimulation paradigms. *Brain Stimul* 7:372–380.
- 958 Lutti A, Dick F, Sereno MI, Weiskopf N (2014) Using high-resolution quantitative mapping of R1 as an
959 index of cortical myelination. *Neuroimage* 93:176–188.
- 960 Lutti A, Hutton C, Finsterbusch J, Helms G, Weiskopf N (2010) Optimization and validation of methods for
961 mapping of the radiofrequency transmit field at 3T. *Magn Reson Med* 64:229–238.
- 962 Maertens De Noordhout A, Rapisarda G, Bogacz D, Gérard P, De Pasqua V, Pennisi G, Delwaide PJ (1999)
963 Corticomotoneuronal synaptic connections in normal man. An electrophysiological study. *Brain*
964 122:1327–1340.
- 965 Nieuwenhuys R (2013) The myeloarchitectonic studies on the human cerebral cortex of the Vogt-Vogt
966 school, and their significance for the interpretation of functional neuroimaging data. *Brain Struct Funct*
967 218:303–352.
- 968 Oldfield RC (1971) The assessment and analysis of handedness: The Edinburgh inventory.
969 *Neuropsychologia* 9:97–113.
- 970 Opitz A, Windhoff M, Heidemann RM, Turner R, Thielscher A (2011) How the brain tissue shapes the
971 electric field induced by transcranial magnetic stimulation. *Neuroimage* 58:849–859.
- 972 Pajevic S, Basser PJ, Fields RD (2014) Role of myelin plasticity in oscillations and synchrony of neuronal
973 activity. *Neuroscience* 276:135–147.
- 974 Palmer E, Ashby P (1992) Corticospinal projections to upper limb motoneurons in humans. *J Physiol*
975 448:397–412.
- 976 Pascual-Leone A, Grafman J, Hallett M (1994) Modulation of cortical motor output maps during
977 development of implicit and explicit knowledge. *Science* (80-) 263:1287–1289.
- 978 Peirce JW (2009) Generating stimuli for neuroscience using PsychoPy. *Front Neuroinform* 2:1–8.
- 979 Peterchev A V., Goetz SM, Westin GG, Luber B, Lisanby SH (2013) Pulse width dependence of motor
980 threshold and input-output curve characterized with controllable pulse parameter transcranial magnetic
981 stimulation. *Clin Neurophysiol* 124:1364–72.

- 982 Picard N, Strick PL (2001) Imaging the premotor areas. *Curr Opin Neurobiol* 11:663–672.
- 983 Pienaar R, Fischl B, Caviness V, Makris N, Grant PE (2008) A methodology for analyzing curvature in the
984 developing brain from preterm to adult. *Int J Imaging Syst Technol* 18:42–68.
- 985 Raffin E, Pellegrino G, Di Lazzaro V, Thielscher A, Siebner HR (2015) Bringing transcranial mapping into
986 shape: Sulcus-aligned mapping captures motor somatotopy in human primary motor hand area.
987 *Neuroimage* 120:164–175.
- 988 Raffin E, Siebner HR (2018) Use-Dependent Plasticity in Human Primary Motor Hand Area: Synergistic
989 Interplay Between Training and Immobilization. *Cereb Cortex* 29:356–371.
- 990 Rathelot J-A, Strick PL (2006) Muscle representation in the macaque motor cortex: An anatomical
991 perspective. *Proc Natl Acad Sci* 103:8257–8262.
- 992 Rathelot J-A, Strick PL (2009) Subdivisions of primary motor cortex based on cortico-motoneuronal cells.
993 *Proc Natl Acad Sci* 106:918–923.
- 994 Rossi S et al. (2009) Safety, ethical considerations, and application guidelines for the use of transcranial
995 magnetic stimulation in clinical practice and research. *Clin Neurophysiol* 120:2008–2039.
- 996 Rossini PM et al. (2015) Non-invasive electrical and magnetic stimulation of the brain, spinal cord, roots and
997 peripheral nerves: Basic principles and procedures for routine clinical and research application: An
998 updated report from an I.F.C.N. Committee. *Clin Neurophysiol* 126:1071–1107.
- 999 Salvador R, Silva S, Basser PJ, Miranda PC (2011) Determining which mechanisms lead to activation in the
1000 motor cortex: A modeling study of transcranial magnetic stimulation using realistic stimulus
1001 waveforms and sulcal geometry. *Clin Neurophysiol* 122:748–758.
- 1002 Sánchez-Panchuelo RM, Francis ST, Schluppeck D, Bowtell RW (2012) Correspondence of human visual
1003 areas identified using functional and anatomical MRI in vivo at 7 T. *J Magn Reson Imaging* 35:287–
1004 299.
- 1005 Sarfeld AS, Diekhoff S, Wang LE, Liuzzi G, Uludağ K, Eickhoff SB, Fink GR, Grefkes C (2012)
1006 Convergence of human brain mapping tools: Neuronavigated TMS Parameters and fMRI activity in the
1007 hand motor area. *Hum Brain Mapp* 33:1107–1123.
- 1008 Seidl AH, Rubel EW, Harris DM (2010) Mechanisms for adjusting interaural time differences to achieve
1009 binaural coincidence detection. *J Neurosci* 30:70–80.

- 1010 Sereno MI, Lutti A, Weiskopf N, Dick F (2013) Mapping the Human Cortical Surface by Combining
1011 Quantitative T1 with Retinotopy†. *Cereb Cortex* 23:2261–2268.
- 1012 Shams Z, Norris DG, Marques JP (2019) A comparison of in vivo MRI based cortical myelin mapping using
1013 T1w/T2w and R1 mapping at 3T. *PLoS One* 14:e0218089.
- 1014 Siebner HR (2020) Does TMS of the precentral motor hand knob primarily stimulate the dorsal premotor
1015 cortex or the primary motor hand area? *Brain Stimul* 13:517–551.
- 1016 Smith S, Jenkinson M, Woolrich MW, Saunders J, Brady JM, Matthews PM, Drobnjak I, Behrens TEJ, De
1017 Stefano N, Jenkinson M, Bannister PR, Flitney DE, Beckmann CF, Zhang Y, Niazky RK, Johansen-
1018 Berg H, Smith SM, Vickers J, De Luca M (2004) Advances in functional and structural MR image
1019 analysis and implementation as FSL. *Neuroimage* 23 Suppl 1:S208-19.
- 1020 Sugiura M, Kawashima R, Takahashi T, Xiao R, Tsukiura T, Sato K, Kawano K, Iijima T, Fukuda H (2001)
1021 Different distribution of the activated areas in the dorsal premotor cortex during visual and auditory
1022 reaction-time tasks. *Neuroimage* 14:1168–1174.
- 1023 Teitti S, Määttä S, Säisänen L, Könönen M, Vanninen R, Hannula H, Mervaala E, Karhu J (2008) Non-
1024 primary motor areas in the human frontal lobe are connected directly to hand muscles. *Neuroimage*
1025 40:1243–1250.
- 1026 Thielscher A, Antunes A, Saturnino GB (2015) Field modeling for transcranial magnetic stimulation: A
1027 useful tool to understand the physiological effects of TMS? In: *Proceedings of the Annual International*
1028 *Conference of the IEEE Engineering in Medicine and Biology Society, EMBS*, pp 222–225.
- 1029 Thielscher A, Kammer T (2004) Electric field properties of two commercial figure-8 coils in TMS:
1030 Calculation of focality and efficiency. *Clin Neurophysiol* 115:1697–1708.
- 1031 Thielscher A, Opitz A, Windhoff M (2011) Impact of the gyral geometry on the electric field induced by
1032 transcranial magnetic stimulation. *Neuroimage* 54:234–243.
- 1033 Timmler S, Simons M (2019) Grey matter myelination. *Glia* 67:2063–2070.
- 1034 Vaalto S, Julkunen P, Säisänen L, Könönen M, Määttä S, Karhu J (2016) Increased Inhibition in Non-
1035 Primary Motor Areas of String-Instrument Players: A Preliminary Study with Paired-Pulse Transcranial
1036 Magnetic Stimulation. *Brain Plast* 1:223–234.
- 1037 Vaalto S, Säisänen L, Könönen M, Julkunen P, Hukkanen T, Määttä S, Karhu J (2011) Corticospinal output

- 1038 and cortical excitation-inhibition balance in distal hand muscle representations in nonprimary motor
1039 area. *Hum Brain Mapp* 32:1692–1703.
- 1040 Veldema J, Bösl K, Nowak DA (2017) Motor Recovery of the Affected Hand in Subacute Stroke Correlates
1041 with Changes of Contralesional Cortical Hand Motor Representation. *Neural Plast* 2017:6171903.
- 1042 Volz LJ, Hamada M, Rothwell JC, Grefkes C (2015) What Makes the Muscle Twitch: Motor System
1043 Connectivity and TMS-Induced Activity. *Cereb Cortex* 25:2346–2353.
- 1044 Ward NS, Bestmann S, Hartwigsen G, Weiss MM, Christensen LOD, Frackowiak RSJ, Rothwell JC, Siebner
1045 HR (2010) Low-Frequency Transcranial Magnetic Stimulation over Left Dorsal Premotor Cortex
1046 Improves the Dynamic Control of Visuospatially Cued Actions. *J Neurosci* 30:9216–9223.
- 1047 Wassermann EM, Pascual-Leone A, Valls-Solé J, Toro C, Cohen LG, Hallett M (1993) Topography of the
1048 inhibitory and excitatory responses to transcranial magnetic stimulation in a hand muscle.
1049 *Electroencephalogr Clin Neurophysiol Evoked Potentials* 89:424–433.
- 1050 Weise K, Numssen O, Thielscher A, Hartwigsen G, Kn TR (2020) A novel approach to localize cortical
1051 TMS effects. *Neuroimage* 209:116486.
- 1052 Weiskopf N, Helms G (2008) Multi-parameter mapping of the human brain at 1mm resolution in less than 20
1053 minutes N. In: *Proceedings of the 16th Scientific Meeting ISMRM*.
- 1054 Weiskopf N, Lutti A, Helms G, Novak M, Ashburner J, Hutton C (2011) Unified segmentation based
1055 correction of R1 brain maps for RF transmit field inhomogeneities (UNICORT). *Neuroimage* 54:2116–
1056 2124.
- 1057 West DC, Wolstencroft JH (1983) Strength-duration characteristics of myelinated and non-myelinated
1058 bulbospinal axons in the cat spinal cord. *J Physiol* 337:37–50.
- 1059 Witham CL, Fisher KM, Edgley SA, Baker SN (2016) Corticospinal inputs to primate motoneurons
1060 innervating the forelimb from two divisions of primary motor cortex and area 3a. *J Neurosci* 36:2605–
1061 2616.
- 1062 Witt ST, Laird AR, Meyerand ME (2008) Functional neuroimaging correlates of finger-tapping task
1063 variations: An ALE meta-analysis. *Neuroimage* 42:343–356.
- 1064 Worsley KJ, Marrett S, Neelin P, Vandal AC, Friston KJ, Evans AC (1996) A unified statistical approach for
1065 determining significant signals in images of cerebral activation. *Hum Brain Mapp* 4:58–73.

1066 Yousry TA, Schmid UD, Alkadhi H, Schmidt D, Peraud A, Buettner A, Winkler P (1997) Localization of the
1067 motor hand area to a knob on the precentral gyrus. A new landmark. *Brain* 120:141–157.

1068 Ziemann U, Siebner HR (2015) Inter-subject and intersession variability of plasticity induction by non-
1069 invasive brain stimulation: Boon or bane? *Brain Stimul* 8:662–663.

1070

1071

1072

1073

1074

1075

1076

1077

1078

1079

1080

1081

1082

1083

1084

1085

1086

1087 **Figure Legends**

1088 **Figure 1**

1089 **Multimodal mapping of the precentral hand knob.**

1090 (A) The top panel illustrates sulcus-aligned mapping with single-pulse transcranial magnetic stimulation
1091 (TMS). The mapping grid consists of five lines with seven target sites per line. The lines follow the
1092 individual shape of the precentral gyrus forming the right precentral hand knob. Single-pulse TMS was
1093 applied at each target site and motor evoked potentials (MEPs) were recorded from left first dorsal

1094 interosseous (FDI) and abductor digiti minimi (ADM) muscles. The first two lines (light blue) corresponded
1095 to posterior lip of the pre-Central Gyrus crown (Pre-CG). The remaining three lines (orange) corresponded
1096 to the top of the Pre-CG crown till the pre-Central Sulcus (Pre-CS). The bottom panel shows colour-coded
1097 corticomotor maps for the FDI and ADM muscle. Each square represents a stimulation site and the colour
1098 codes the mean MEP amplitude. Note that the FDI muscle is represented more laterally respect to the ADM
1099 muscle. B) Surface-rendered group map of the simulated electric field strength induced by TMS. (C)
1100 Structural MRI: Average distribution of cortical thickness (top) and cortical myelination (bottom)
1101 measured as longitudinal relaxation rate $R1 = 1/T1$ across all subjects. (D) Average fMRI activity for
1102 voluntary abduction-adduction movements of the left index (FDI) and little (ADM) fingers during a visually
1103 cued motor task at 1 Hz.

1104

1105 **Figure 2**

1106 **Structural, functional and electrical field properties of the right precentral gyrus (Pre-CG).**

1107 (A) The left panel represents the right precentral Region of Interest (ROI) considered for the analyses,
1108 namely the light blue mask including the gyral wall facing the Central Sulcus (CS), caudal pre-CG ROI, and
1109 the orange mask composed of the gyral crown and gyral wall facing the pre-Central Sulcus (pre-CS), rostral
1110 pre-CG ROI. Bottom figure indicates the cross section (following the blue dotted line) of Pre-CG with a
1111 schematic representation of caudal pre-CG and rostral pre-CG ROIs. (B-E) Significant differences are
1112 evident between the caudal pre-CG and rostral pre-CG ROIs regarding the cortical myelin content (B),
1113 functional activation during the visually cued movement repetition task (C), mean cortical thickness (D) and
1114 mean TMS-induced field strength (E). Each panel consists of a bar-plot representing the regional mean
1115 (left) and a surface-rendered voxel-wise group map, including the borders of the two ROIs.

1116

1117 **Figure 3**

1118 **Corticomotor maps of the right precentral hand knob derived from sulcus-shape based TMS**
1119 **mapping.**

1120 (A) Two-dimensional colour-coded map illustrating the spatially distribution of corticomotor excitability in
1121 the right precentral hand knob. The motor hotspot is indicated by an "X". The left panel shows the map of

1122 an individual (subject n. 3) with caudal hotspot location in the posterior lip of the precentral gyrus for the
1123 FDI muscle (upper panel) and ADM muscle (lower panel). The right panel shows the map of an individual
1124 (subject n. 18) with a more rostral hot spot at the top of the precentral crown. Each square corresponds to a
1125 specific target site determined by its medio-lateral (target 1 to 7) and posterior-anterior position (lines 1-5).
1126 (B) Scatter plots plotting the x (medio-lateral direction) or y (posterior-anterior direction) coordinates of the
1127 motor hot spot in MNI space against the shortest MEP latency recorded at the motor hot spot location.
1128 Significant correlations with MEPs latencies were only found for the posterior-anterior position of the
1129 hotspot coordinates (y-coordinates) but not for medio-lateral position (x-coordinates). Open black circles
1130 indicate participants with a more caudal hot spot location in the posterior lip of Pre-CG (located on lines 1
1131 and 2 of the mapping grid). Close black circles indicate participants with a more rostral hot spot location at
1132 the top of the Pre-CG crown (located on line 3 or 4 of the mapping grid). Please, note that the labelling of
1133 the x-axes is identical for all four scatter plots.

1134

1135 **Figure 4**

1136 **A higher cortical myelin content in right precentral motor hand knob is associated with a more**
1137 **rostral hot-spot location**

1138 Positive linear relationship between cortical myelination (as indexed by the mean R1 signal) in the
1139 precentral hand knob and the spatiotemporal rostrality index of the TMS hot-spot for the FDI (A) and ADM
1140 muscle (C). Open and close black circles indicate subjects with hotspot located in the posterior lip of
1141 precentral crown and top of the precentral crown, respectively.

1142 Surface-rendered statistical parametric maps: The maps show voxels with a significant positive relationship
1143 between the precentral myelin-related signal and rostrality index for FDI (B) and ADM hot spot (D).

1144 Pre-CG: Pre-Central Gyrus; ROI: Region of interest, FDI: first dorsal interosseous; ADM= abductor digiti
1145 minimi.

1146

1147 **Figure 5**

1148 **A higher cortical myelin content in right precentral motor hand knob is associated with a higher**
1149 **functional activation during visually cued repetitive finger movements**

1150 Positive linear relationship between cortical myelination (as indexed by the mean R1 signal) in the
1151 precentral hand knob and the BOLD signal increase during the visuo-motor abduction task. The same
1152 positive relationship became evident when the task was performed with the left index finger (A) or little
1153 finger (C). Open and close black circles indicate subjects with hotspot located in the posterior lip of
1154 precentral crown and top of the precentral crown, respectively. Surface-rendered statistical parametric
1155 maps: The maps show voxels with a significant positive relationship between the precentral myelin-related
1156 signal and the task-related BOLD increase for index (B) and little finger (D). Pre-CG: Pre-Central Gyrus;
1157 ROI: Region of interest.

1158

1159 Figure 6**1160 Relationship between the cortical myelin content in right precentral motor hand knob and temporal
1161 synchronization of repetitive finger movements.**

1162 Negative linear relationship between cortical myelination (as indexed by the mean R1 signal) in the
1163 precentral hand knob and the coefficient of variation of the inter-movement interval during the visuo-motor
1164 abduction task. The same negative relationship became evident when the task was performed with the left
1165 index finger (A) or little finger (C). Open and close black circles indicate subjects with hotspot located in
1166 the posterior lip of precentral crown and top of the precentral crown, respectively.
1167 Surface-rendered voxel-wise correlation maps indicating a negative relationship between precentral cortical
1168 myelination and the coefficient of variation of the inter-movement interval during the visuo-motor
1169 abduction task and for the index (B) and little finger (D). Statistical maps are thresholded at $p_{\text{uncorr}} < 0.01$ for
1170 illustrative purposes. Pre-CG: Pre-Central Gyrus; ROI: Region of interest.

1171

1172 Figure 7**1173 Simulations of the electric field strength induced by TMS at motor hotspot location.**

1174 Colour-coded surface-rendered group maps for participants with preferential hotspot location in the
1175 posterior lip of the precentral gyrus (A) or at the top of the precentral crown (B). The surface-based
1176 statistical map (C) shows a single cluster in the posterior lip of the precentral gyrus where participants with
1177 preferential hotspot location in the posterior lip of the Pre-Central Gyrus crown display a higher electrical

1178 field strength than participants with a more rostral location of motor hotspot. Between-groups difference of
1179 the mean electric field strength extracted from the significant cluster in the posterior lip region (D) . Mean
1180 electrical field strength in this cluster is higher in subjects with a more posterior motor hotspot location in
1181 the precentral crown (white column) than in subjects with a more rostral motor hotspot location (black bar),
1182 * $t_{(16,7)} = 2.604$, $p = 0.019$; unpaired t-test.

1183

1184 **Table 1**

1185 **The table lists demographic and electrophysiological data (mean±SEM)**

1186 RMT = Resting motor threshold; %MSO= percentage of maximum stimulation output; MEP = Motor evoked
1187 potential; FDI= first dorsal interosseous; ADM= abductor digiti minimi. The p-values refer to between-group
1188 comparisons comparing mean values of variables (Caudal hotspot group vs Rostral hotspot group).

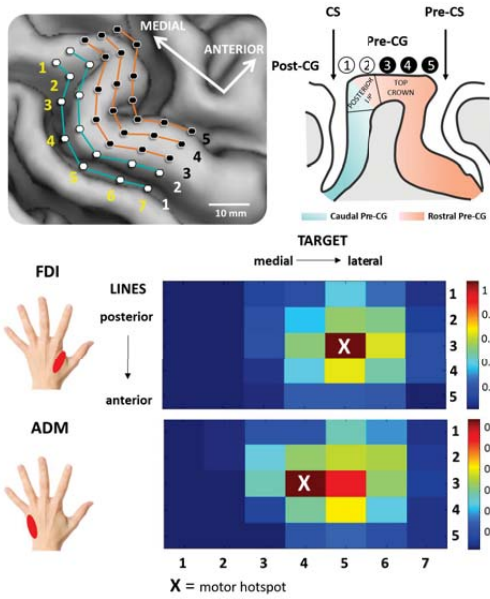
1189

1190

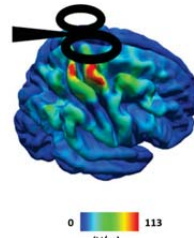
1191

1192

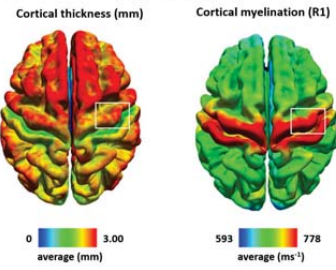
A Sulcus-aligned TMS mapping of corticomotor representation



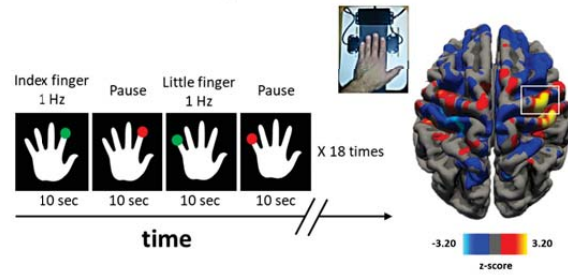
B Electric field modelling

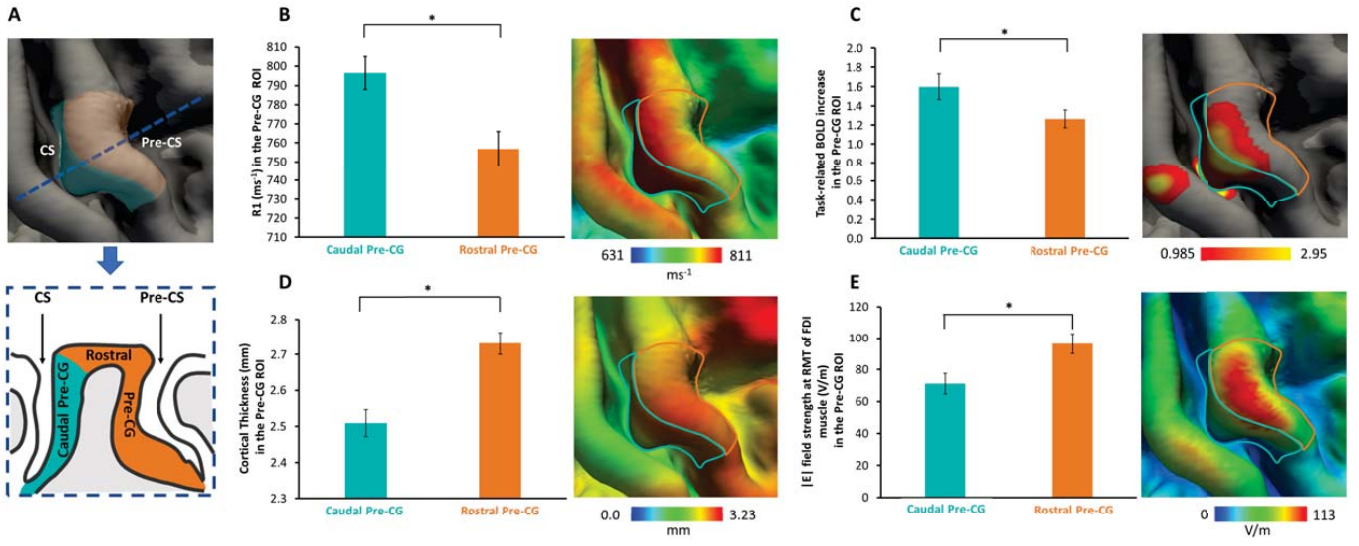


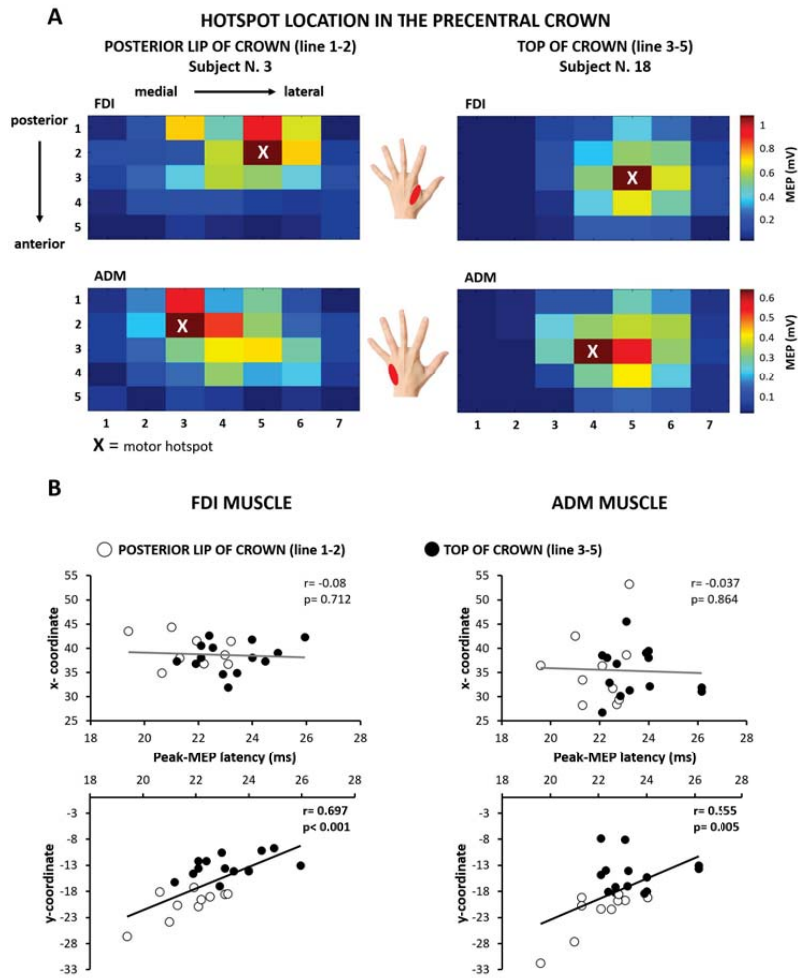
C Structural MRI

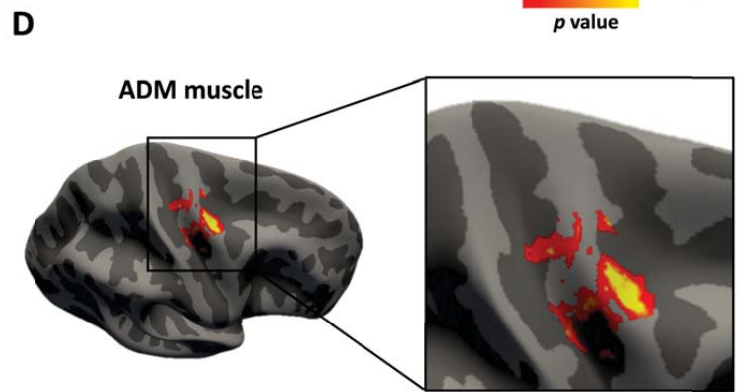
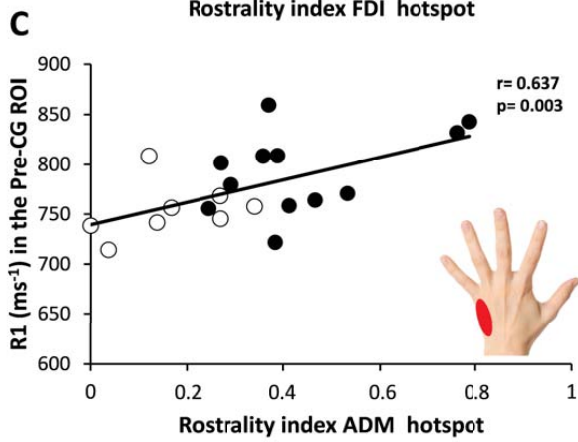
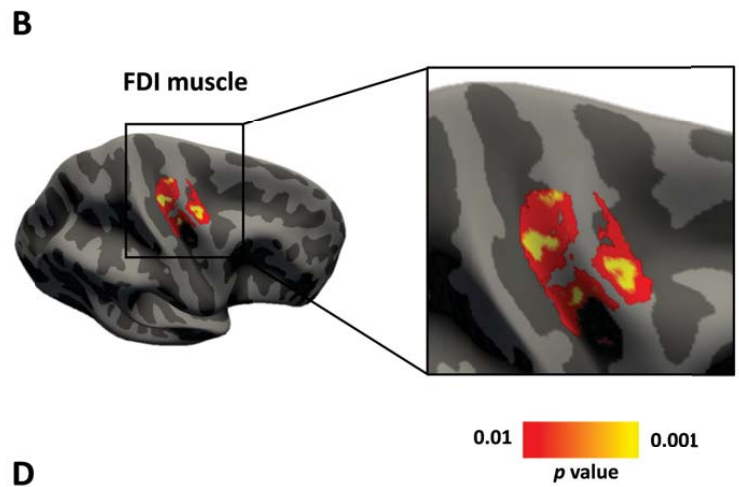
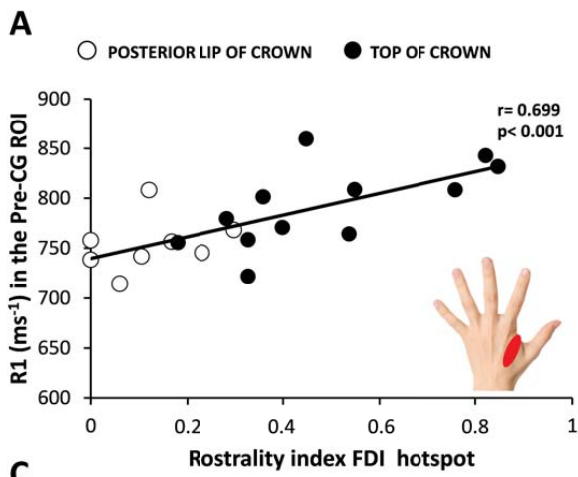


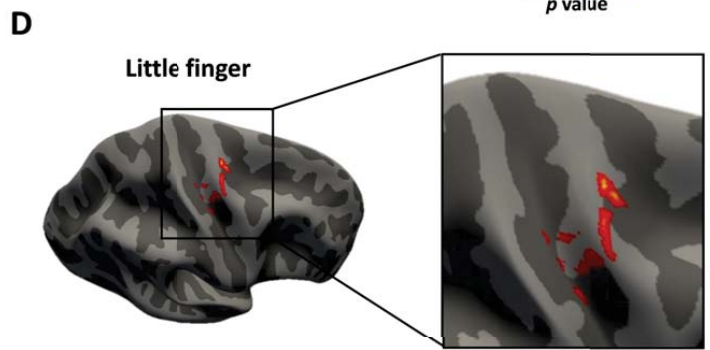
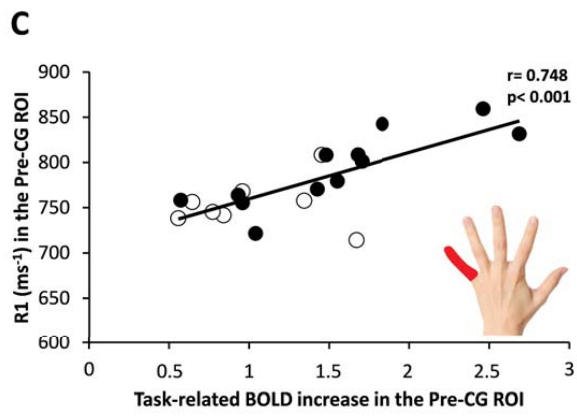
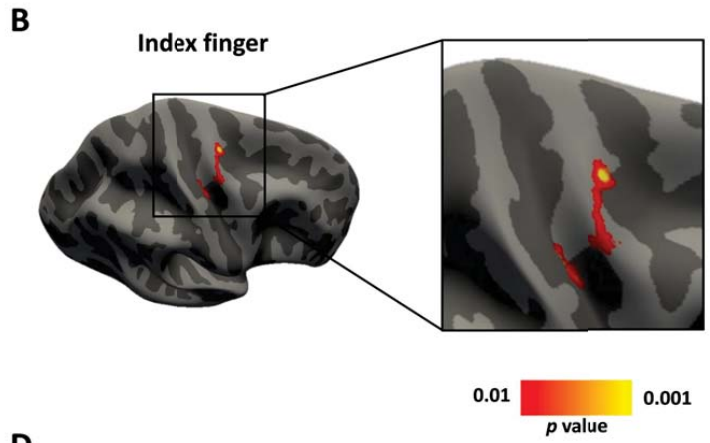
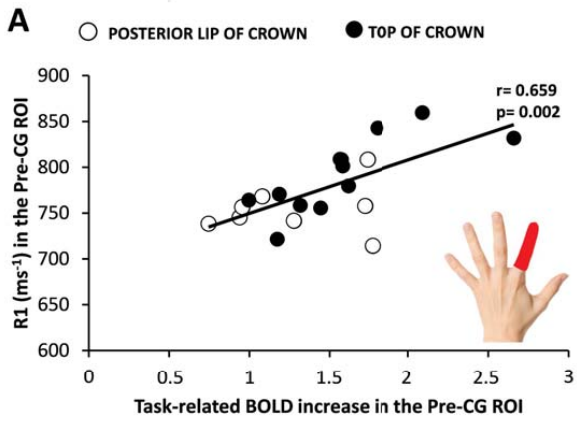
D Functional MRI during a visuo-motor synchronization task

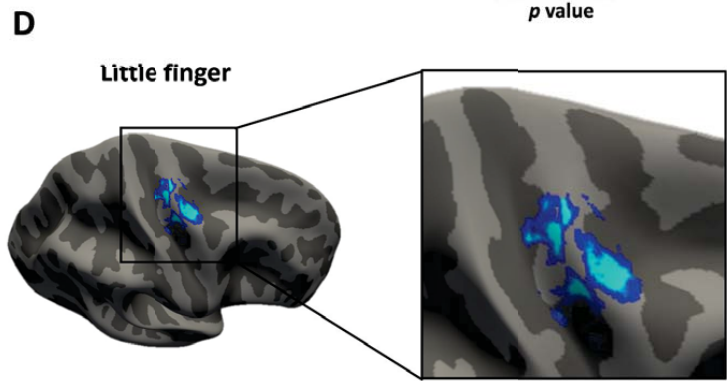
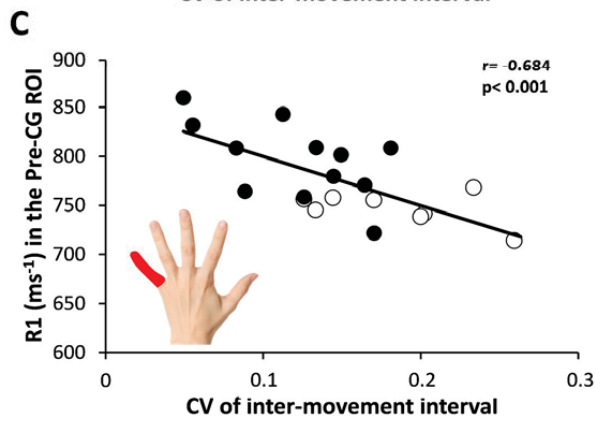
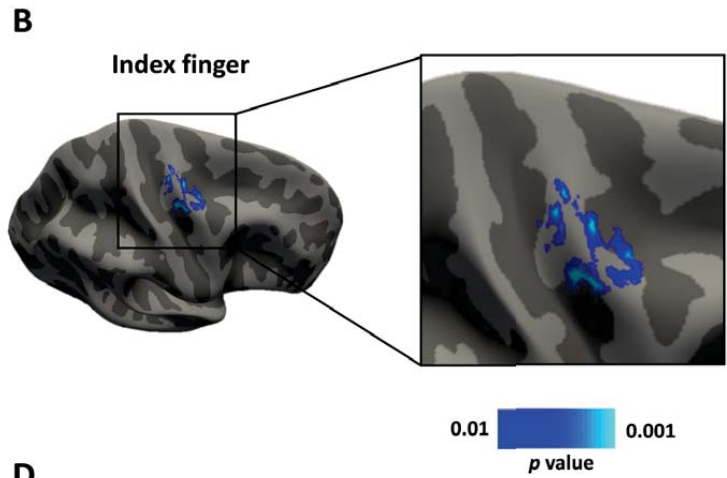
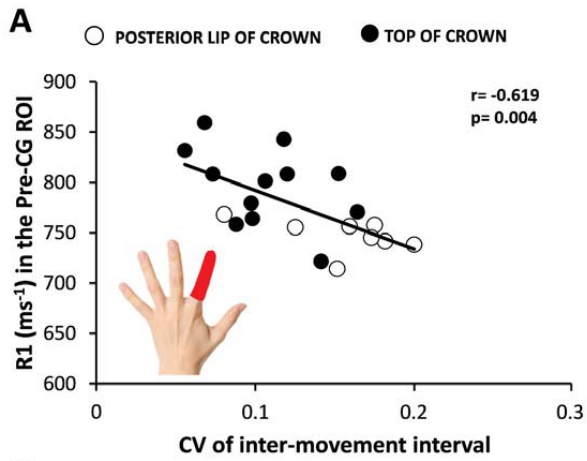


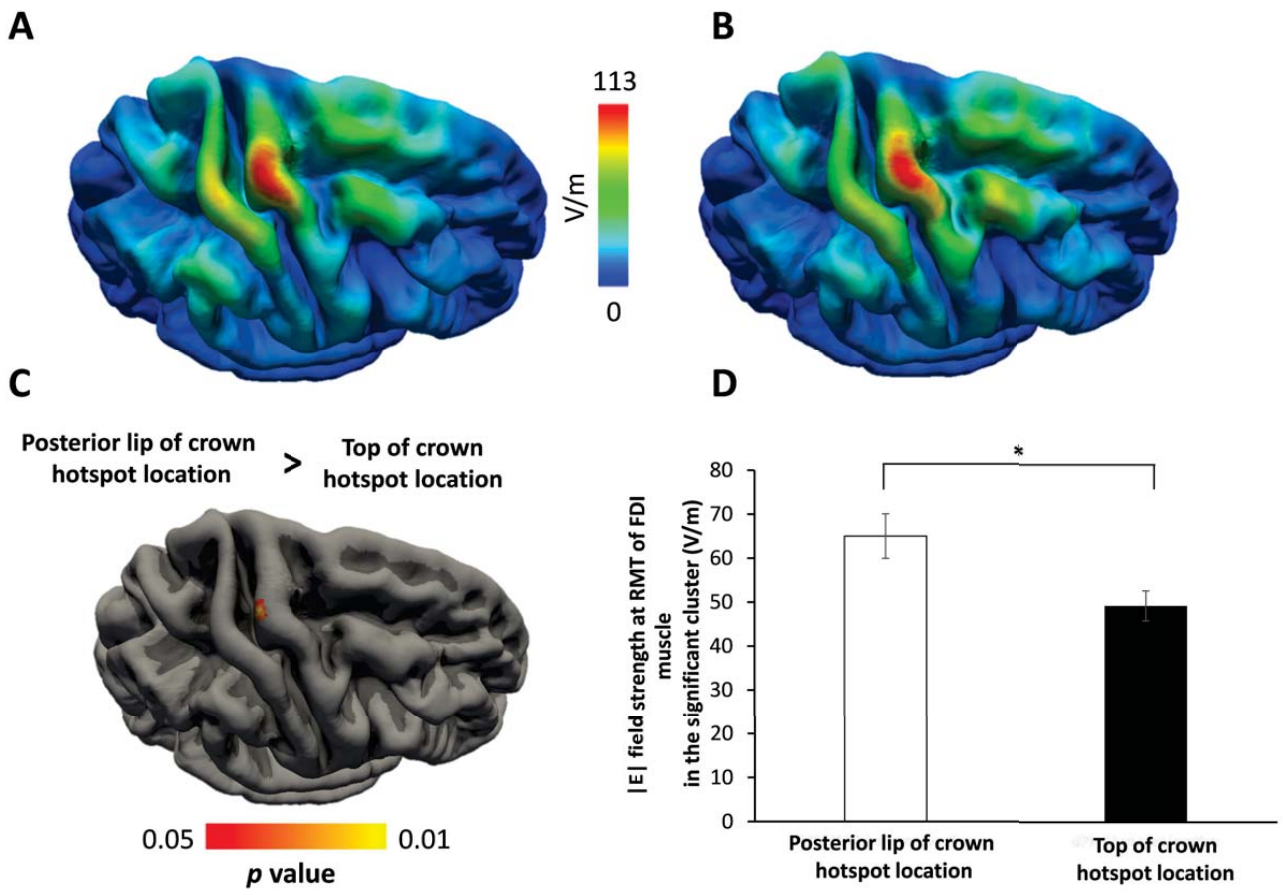












| | All participants (n=24) | Caudal hotspot group (n=10) | Rostral hotspot group (n=14) | Statistic, p-value |
|---|-------------------------|-----------------------------|------------------------------|-------------------------------------|
| Sex (Male/Female) | 12/12 | 5/5 | 7/7 | $\chi^2 = 0$, p=1 |
| Age (Years) | 24.2 ± 0.9 | 22.6 ± 1.1 | 25.4 ± 1.3 | $t_{(22)} = -1.699$, p= 0.11 |
| Height (cm) | 172.9 ± 6.0 | 171.5 ± 4.7 | 173.9 ± 6.8 | $t_{(22)} = -1.004$, p= 0.326 |
| RMT of FDI muscle (% MSO) | 58.1 ± 2.2 | 55.3 ± 2.4 | 60.1 ± 3.4 | $t_{(21.6)} = -1.144$, p= 0.27 |
| MEP latency at hotspot (ms) | | | | |
| Left FDI muscle | 22.6 ± 0.3 | 21.7 ± 0.4 | 23.3 ± 0.4 | $t_{(20.9)} = -2.952$, p= 0.008 |
| Left ADM muscle | 22.9 ± 0.3 | 22.0 ± 0.4 | 23.5 ± 0.4 | $t_{(21.1)} = -3.033$, p= 0.006 |
| MEP Amplitude at hotspot (mV) | | | | |
| Left FDI muscle | 1.1 ± 0.2 | 1.3 ± 0.3 | 1.0 ± 0.2 | $t_{(14.46)} = 0.804$, p= 0.43 |
| Left ADM muscle | 0.5 ± 0.1 | 0.4 ± 0.1 | 0.6 ± 0.1 | $t_{(21.6)} = -0.682$, p= 0.5 |
| MNI-coordinates of motor hotspot | | | | |
| Left FDI muscle (x-coordinate) | 38.7 ± 0.6 | 39.4 ± 1.0 | 38.1 ± 0.8 | $t_{(19.1)} = 1.02$, p= 0.32 |
| Left FDI muscle (y-coordinate) | -16.6 ± 1.0 | -21.3 ± 1.2 | -13.2 ± 0.6 | $t_{(13)} = -6.11$, p= <0.001 |
| Left FDI muscle (z-coordinate) | 66.5 ± 0.6 | 65.2 ± 0.9 | 67.4 ± 0.7 | $t_{(16)} = -1.873$, p= 0.08 |
| Left ADM muscle (x-coordinate) | 35.4 ± 1.2 | 35.8 ± 2.4 | 35.1 ± 1.3 | $t_{(14.35)} = 0.269$, p= 0.79 |
| Left ADM muscle (y-coordinate) | -17.8 ± 1.1 | -21.7 ± 1.4 | -15.0 ± 1.0 | $t_{(16.7)} = -3.85$, p= 0.001 |
| Left ADM muscle (z-coordinate) | 69.1 ± 1.0 | 67.8 ± 1.6 | 70.1 ± 1.3 | $t_{(18.8)} = -1.113$, p= 0.28 |
| Spatiotemporal rostrality index | | | | |
| Left FDI muscle | 0.34 ± 0.05 | 0.14 ± 0.03 | 0.49 ± 0.05 | $t_{(15.6)} = -6.568$, p <0.001 |
| Left ADM muscle | 0.32 ± 0.04 | 0.18 ± 0.03 | 0.42 ± 0.05 | $t_{(16.7)} = -3.850$, p <0.001 |

Table 1.

The table lists demographic and electrophysiological data (mean±SEM)

RMT = Resting motor threshold; %MSO= percentage of maximum stimulation output; MEP = Motor evoked potential; FDI= first dorsal interosseous; ADM= abductor digiti minimi. The p-values refer to between-group comparisons comparing mean values of variables (Caudal hotspot group vs Rostral hotspot group).